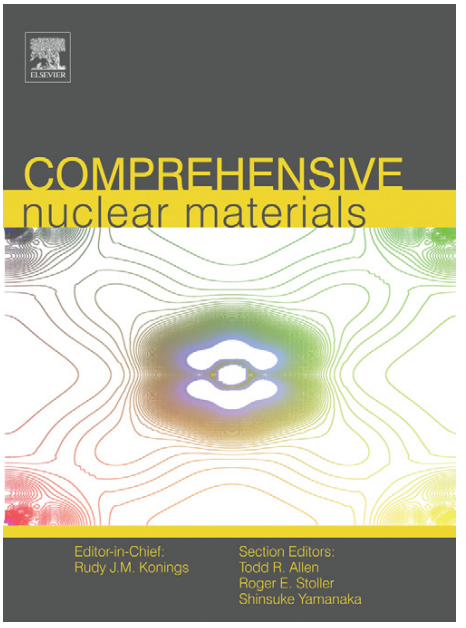

Li M. and Zinkle S.J. (2012) Physical and Mechanical Properties of Copper and Copper Alloys. In: Konings R.J.M., (ed.) Comprehensive Nuclear Materials, volume 4, pp. 667-690 Amsterdam: Elsevier.

4.20 Physical and Mechanical Properties of Copper and Copper Alloys

M. Li
Argonne National Laboratory, Argonne, IL, USA
S. J. Zinkle
Oak Ridge National Laboratory, Oak Ridge, TN, USA

Published by Elsevier Ltd.

Abbreviations

CW	Cold worked
DS	Dispersion strengthened
FFTF	Fast Flux Test Facility
G-P	Guinier–Preston
HIP	Hot isostatic pressing
IACS	International Annealed Copper Standard
JET	Joint European Torus
MOTA	Materials Open Test Assembly
OFHC	Oxygen-free, high conductivity
PH	Precipitation hardened
SAA	Solution annealed, and aged condition
SFT	Stacking fault tetrahedral
TCH	Tension and compression hold

4.20.1 Introduction

Copper alloys are prime candidates for high heat flux applications in fusion energy systems. High heat flux is a major challenge for various fusion devices because of the extremely high energy density required in controlled thermonuclear fusion. The removal of a large amount of heat generated in the plasma through

Comprehensive Nuclear Materials (2012), vol. 4, pp. 667-690

the first wall structure imposes a major constraint on the component design life. Materials with high conductivity are needed to assist heat transfer to the coolant and to reduce the thermal stress for pulsed mode of operation.

A number of issues must be considered in the selection of materials for high heat flux applications in fusion reactors. While high conductivity is the key property for such applications, high strength and radiation resistance are also essential for the effective performance of materials in a high heat flux, high irradiation environment. In addition, fatigue behavior is a major concern for many high heat flux applications because of planned or inadvertent changes in the thermal loading. Pure copper has high thermal conductivity but rather low strength, and therefore its application as heat sinks is limited. The strength of copper can be improved by various strengthening mechanisms. Among them, precipitation hardening and dispersion strengthening are the two most viable mechanisms for improving the strength of copper while retaining its high electrical and thermal conductivities. A number of precipitation-hardened (PH) and dispersion-strengthened (DS) copper alloys are commercially available, and have been evaluated for fusion applications, for example, PH CuCrZr, CuNiBe, CuNiSi, and DS GlidCop® Al15, Al25, Al60, MAGT-0.2, etc. Two copper alloys that are most appealing are PH CuCrZr and DS CuAl25. Surveys of copper alloys for fusion applications were conducted by Butterworth and Forty[1] and Zinkle and Fabritsiev.[2]

In this chapter, a brief description of pure copper and several copper alloys of interest to fusion applications is presented, followed by a summary of their physical and mechanical properties. The radiation effects on the physical and mechanical properties of copper and copper alloys as well as their irradiated microstructure are then discussed. Joining techniques for plasma facing components in fusion reactors are also discussed.

4.20.2 Copper and High-Strength, High-Conductivity Copper Alloys

4.20.2.1 Pure Copper

Copper is widely used where high electrical or thermal conductivity is required. Pure copper is defined as having a minimum copper content of 99.3%. Copper with oxygen content below 10 ppm is called 'oxygen-free.' 'Oxygen-free, high conductivity' (OFHC) grade copper has room temperature electrical conductivities equal to or greater than 100% International Annealed Copper Standard (IACS), where 100% IACS = 17.241 nΩ m at 20 °C.[3] Copper grades with the ASTM/SAE unified number system (UNS) designation C10100, C10200, C10400, C10500, and C10700 are classified as OFHC copper. Grades C10400, C10500, and C10700 have significant silver content, which creates activation hazards. Only C10100 and C10200 are considered for fusion systems.

The use of unalloyed copper is often limited by its low strength. Copper can be strengthened by various processes, for example, cold working, grain refinement, solid solution hardening, precipitation hardening, dispersion strengthening, etc. While these approaches can significantly increase the strength, they can also lead to a pronounced reduction in conductivity. The challenge is to design a material with the best combination of strength and conductivity.

Cold work can significantly increase the strength of pure copper and has a relatively moderate effect on conductivity.[4] However, cold-worked copper can be softened at relatively low temperatures (~200 °C) because of its low recrystallization temperature.[5] A recent study has shown that ultrahigh-strength and high-conductivity copper can be produced by introducing a high density of nanoscale twin boundaries.[6] The tensile strength of the nano-grained copper can be increased by a factor of 10 compared to conventional coarse-grained copper, while retaining a comparable conductivity. The potential of high-strength, high-conductivity bulk nano-grained copper in nuclear energy systems, however, has not been widely explored.

Alloying in copper can significantly improve mechanical strengths and raise the softening temperatures. However, additions of alloying elements also reduce electrical and thermal conductivity. Among the three alloying strengthening mechanisms, namely, solid solution hardening, precipitation hardening, and dispersion strengthening, solid solution hardening has the most detrimental effects on the conductivity[4] and is the least favored mechanism to obtain high-conductivity, high-strength copper alloys.

4.20.2.2 PH Copper Alloys

PH copper alloys are heat-treatable alloys. The high strength of PH copper alloys is attributed to the uniform distribution of fine precipitates of second-phase particles in the copper matrix. PH copper alloys are produced by conventional solution treatment

and aging treatment. Solution treatment produces a homogeneous solid solution by the heating of an alloy to a sufficiently high temperature to dissolve all solutes. The alloy is then quenched to a lower temperature to create a supersaturated condition. A subsequent aging treatment heats the alloy to an intermediate temperature below the solvus temperature, to precipitate fine second-phase particles. Precipitates not only give rise to high strength, but also reduce the solute content in the matrix, maintaining good conductivity. The strength of a PH alloy depends on particle size, particle shape, volume fraction, particle distribution, and the nature of the interphase boundary.[7] Despite their ability to develop significant strength, PH copper alloys may be softened substantially as a result of precipitation coarsening (overaging) at intermediate to high service temperatures or because of recrystallization during brazing or diffusion bonding. Therefore, heat treatment and thermal processing histories can have a large influence on the strength and conductivity of this class of alloys.

A number of commercial PH copper alloys have been investigated for applications in fusion design, for example, CuCrZr, CuNiBe, and CuNiSi.

4.20.2.2.1 CuCrZr alloy

PH CuCrZr alloy is commercially available under several trade names, for example, Elbrodur® CuCrZr from KME Germany AG, Outokumpu Oy CuCrZr, Zollen CuCrZr, C18150®, Trefimetaux CuCrZr, MATTHEY 328® from Johnson Matthey Metals, and YZC® from Yamaha Co, Ltd. The chemical compositions of these alloys differ by a small amount, with Cr varying from 0.4 to 1.5% and Zr 0.03–0.25%. Low Cr content is to prevent the formation of coarse Cr precipitates. The element, Zr, improves the hardening by the enhancement of fine homogeneous precipitation and improves the ductility of the alloy by inhibiting intergranular fracture.[8–10] CuCrZr-IG is the ITER grade with tighter specification for composition and heat treatment. CuCrZr alloys are available in different forms, for example, bars, tubes, wires, foils, sheets, and plates. Hot forming, brazing, and inert gas welding are applicable for component manufacturing.

CuCrZr alloys are used in the conventional aged condition. The reference ITER heat treatment includes solution annealing at 980–1000 °C for 1 h, water quench, and aging at 450–480 °C for 2–4 h.[11] Typical microstructure of the prime-aged CuCrZr is shown in **Figure 1(a)**. The alloy contains an equiaxed grain structure and uniformly distributed fine Guinier–Preston (GP) zones exhibiting primarily black dot contrasts and a small number of precipitates with lobe–lobe contrast. The number density of precipitates is on the order $10^{22}\,m^{-3}$, with a mean diameter of ~3 nm. A low density of micron-size Cr particles and grain boundary precipitate-free zones were also observed.[12–18] CuCrZr is susceptible to overaging and recrystallization during prolonged exposure at elevated temperatures. Overaging of CuCrZr causes significant coarsening of grain structure and fine precipitates. Li *et al.*[14] reported a lower number density ($\sim 1.9 \times 10^{22}\,m^{-3}$) of larger (~9 nm in diameter) precipitates with a mixture of coherent and incoherent particles after CuCrZr was hot isostatic pressing (HIP) treated at 1040 °C for 2 h at 140 MPa followed by solutionizing at 980 °C for 0.5 h with a slow cooling rate of 50–80 °C min^{-1} between 980 and 500 °C, and final aging at 560 °C for 2 h (**Figure 1(b)**). The average grain size was >500 μm in comparison with ~27 μm grain size in the prime-aged alloy.

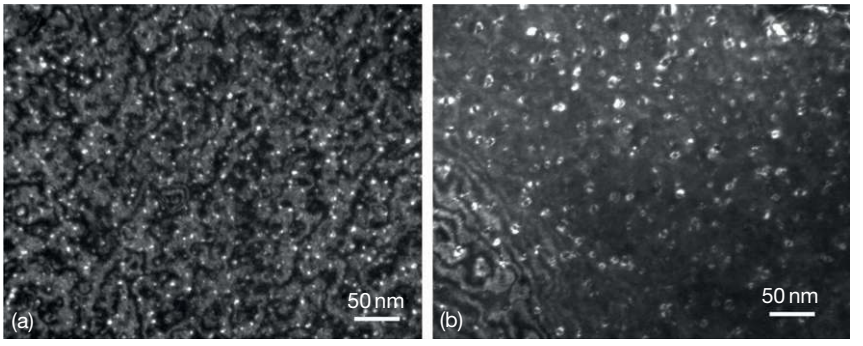

Figure 1 Representative weak-beam dark-field images showing precipitates in unirradiated CuCrZr (a) solutionized, water quenched, and aged, and (b) hot isostatic pressed, solutionized, slow-cooled, and aged.

4.20.2.2.2 CuNiBe alloy

Copper–beryllium (<1 wt% Be) binary alloys provide a good combination of strength and conductivity. The precipitation of Cu–Be binary alloys occurs in both continuous and discontinuous modes. Continuous precipitation creates uniformly distributed fine particles in the copper matrix, as a result of the following precipitation process[19]:

$$\alpha_0(\text{supersaturated}) \rightarrow \text{GP zones} \rightarrow \gamma'' \rightarrow \gamma' \rightarrow \gamma(\text{CuBe})$$

The sequence and morphology of precipitation depends mainly on aging temperature. The first phase to nucleate from a supersaturated Cu–Be solid solution is coherent Cu-rich GP zones. Following the GP zones formation is the precipitation of so-called transition phases, γ'' and γ'. The equilibrium phase, γ, forms after the transition phases, and its appearance indicates overaging of the alloy. Discontinuous precipitation in Cu–Be binary alloys leads to nonuniform precipitation of long, lamellar precipitates, resulting in cell structure at grain boundaries, which increases the tendency to intergranular fracture in the alloy.

High-conductivity Cu–Be alloys generally contain a third element. The addition of a small amount of nickel to Cu–Be binary alloys further increases the strength of the alloys without degrading electrical and thermal conductivities. The addition of nickel increases the precipitate solvus temperatures of Cu–Be binary alloys.[20] A higher solute supersaturation condition can be reached in the solution treatment which provides a larger driving force for precipitation during the aging treatment. The strength of ternary Cu–Ni–Be alloys, therefore, is significantly increased from enhanced precipitation hardening. The electrical and thermal conductivities of Cu–Ni–Be alloys are also increased because of the depletion of the alloying elements from the solid solution during aging, resulting in high strength and high conductivity. CuNiBe exhibits very high strength with respect to other PH copper alloys. The drawback of this alloy is its very low ductility and low fracture toughness after low-dose irradiation.

4.20.2.2.3 CuNiSi

CuNiSi is another PH copper alloy that has been considered for fusion applications. CuNiSi has a nominal composition of 2.5% Ni and 0.6% Si. When heat treated properly, CuNiSi can have a much higher yield strength and higher electrical resistivity than CuCrZr. It has been extensively used for the Joint European Torus (JET) components, for example, the divertor cryopump, the water-cooled baffles, and the Lower Current Hybrid Drive cryopump.[21]

4.20.2.3 DS Copper Alloys

DS copper alloys contain a fine dispersion of nanometer-sized oxide particles such as alumina, zirconia, hafnia, or chromia in the copper matrix, giving rise to high-strength and thermal stability of the alloys. This class of copper alloys can be manufactured by either conventional powder metallurgy or internal oxidation. Their properties strongly depend on the type, dimension, and volume fraction of the dispersed phase and processing techniques. Unlike PH copper alloys, the addition of finely dispersed oxide particles into the copper matrix can prevent recrystallization of the matrix and consequent softening even after exposure to temperatures approaching the melting point of the copper matrix. In addition, the oxide particles are insoluble in the solid state, and are essentially immune to coarsening because of their high melting point and high thermodynamic stability. This extends the useful temperature range of a DS alloy far beyond that possible for conventional PH alloys.

Several DS copper alloys have been evaluated for fusion applications, for example, GlidCop® Al15, Al25, Al60, and MAGT 0.2. Both GlidCop® and MAGT class alloys are strengthened by Al_2O_3 particles, produced by internal oxidation. GlidCop® Al25 and MAGT-0.2 have been studied extensively because of their balanced strength, thermal conductivity, and ductility. GlidCop® Al25 (0.25 wt% Al) is produced by OMG America. CuAl25-IG is the ITER grade with the optimized fabrication process for improved ductility and reduced anisotropy. The microstructure of the CuAl25 alloy is characterized by elongated grain structure along the extrusion or rolling direction and a high density (average of $3.27 \times 10^{22}\,\text{m}^{-3}$) of dispersed Al_2O_3 particles with a mean diameter of 6–9 nm. The distribution of alumina particles can be highly heterogeneous, with some grains free of strengthening particles. A low number density of micron-size α-Al_2O_3 particles exists at grain boundaries. The density of dislocations in the as-wrought condition can be as high as $\sim 1.5 \times 10^{15}\,\text{m}^{-2}$.[15–18,22–24] Most of the oxide particles in GlidCop alloys are triangular platelets with the remainder in the form of circular or irregular-shaped disks.[25]

MAGT 0.2 is a Russian alloy produced by SPEZS-PLAV Company. It contains 0.17% Al, 0.05% Hf, and 0.09% Ti in the form of oxide particles.[25,26] GlidCop contains Al-oxide particles only, while in MAGT alloy, there are Al-, Ti-, and Hf-oxide particles, and mixed Al- and Ti-oxide particles. A majority of the oxide particles in MAGT 0.2 are spherical in shape with a small fraction in the form of circular disks, with an average particle size of 6 nm.[25,26]

4.20.3 Physical Properties of Copper and Copper Alloys

Physical properties of pure copper and copper alloys are quite similar in terms of the melting point, the density, the Young's modulus, and the thermal expansion coefficient. **Table 1** compares the room temperature physical properties of pure copper, PH CuCrZr, and DS CuAl25.[2,27–29] Because PH copper alloys and DS copper alloys contain only a small amount of fine second-phase particles, the physical properties of these copper alloys closely resemble those of pure copper.

The conductivity of copper and copper alloys is the most important physical property for their applications. The electrical conductivity of copper can be reduced by thermal vibration of atoms and crystal imperfections, for example, solute atoms, vacancies, dislocations, and grain boundaries. These different mechanisms have additive contributions to the increase in resistivity. As with other metals, the thermal conductivity of copper, k_{th}, is proportional to the electrical conductivity, λ, described by the Wiedemann–Franz law, that is,

$$k_{th} = \lambda L T \qquad [1]$$

where T is the absolute temperature and L is the Lorentz number. The electrical conductivity of pure copper is sensitive to temperature, and less sensitive to the amount of cold work and the grain size. The linear temperature coefficient for electrical resistivity in copper is $d\rho/dT = 6.7\times10^{-11}\,\Omega\,m\,K^{-1}$.[30] Severe cold work can reduce the electrical conductivity of copper by only 2–3% IACS.

All alloying elements in copper reduce the electrical conductivity, and the amount of degradation depends on the type of element, the concentration, and microstructural form (e.g., solid solution, precipitation, or dispersion). **Figure 2** compares the strength and conductivity of copper and several types of copper alloys.[31]

Table 1 Physical properties of pure copper, PH CuCrZr, and DS CuAl25

	Cu	*CuCrZr*	*CuAl25*
Melting point (°C)	1083	1075	1083
Density (g cm^{-3})	8.95	8.90	8.86
Thermal conductivity (W m-K^{-1})	391	314–335	364
Elastic modulus (GPa)	117	123	130

4.20.4 Mechanical Properties of Copper and Copper Alloys

4.20.4.1 Tensile Properties

The influence of test temperature, strain rate, and thermal–mechanical treatments on the tensile properties of copper and copper alloys has been studied extensively. **Figure 3** illustrates the effect of test temperature on the yield strength of pure copper (in the annealed condition), PH CuCrZr and CuNiBe alloys, and DS CuAl25.[15–18,28,32–39] The strength of copper alloys decreases with increasing test temperature. The decrease in strength is moderate up to 200 °C. Significant drops in strength occur at higher temperatures, except that the CuNiBe AT alloy shows a relatively small reduction in strength even up to 400 °C. Pure copper has the lowest yield strength. The tensile properties of pure copper strongly depend on the thermal–mechanical treatment and the impurity content.[15–18,32,33] CuNiBe alloy has the highest strength over the entire temperature range.[34] The tensile properties of PH copper alloys are sensitive to the thermal–mechanical treatments. CuCrZr in the solution-annealed, cold-worked, and aged condition (SA + CW + A) has superior yield strength at low temperatures relative to CuCrZr in the solution-annealed, and aged condition (SAA). However, the strength of CuCrZr SA + CW + A alloy drops more rapidly with increasing temperature.[29,34–39] The yield strength of CuNiBe can be quite different, depending on the processing techniques. The tensile ductility of copper alloys also shows strong temperature dependence. The uniform elongation of the CuAl25 alloy decreases considerably as the test temperature increases, but increases with increasing test temperature above 400 °C. The CuNiBe AT alloy shows a moderate drop of uniform elongation below 200 °C, but a sharp drop in ductility at higher temperature.[34] The uniform elongation of the CuCrZr alloy shows the smallest sensitivity to test temperature. Among

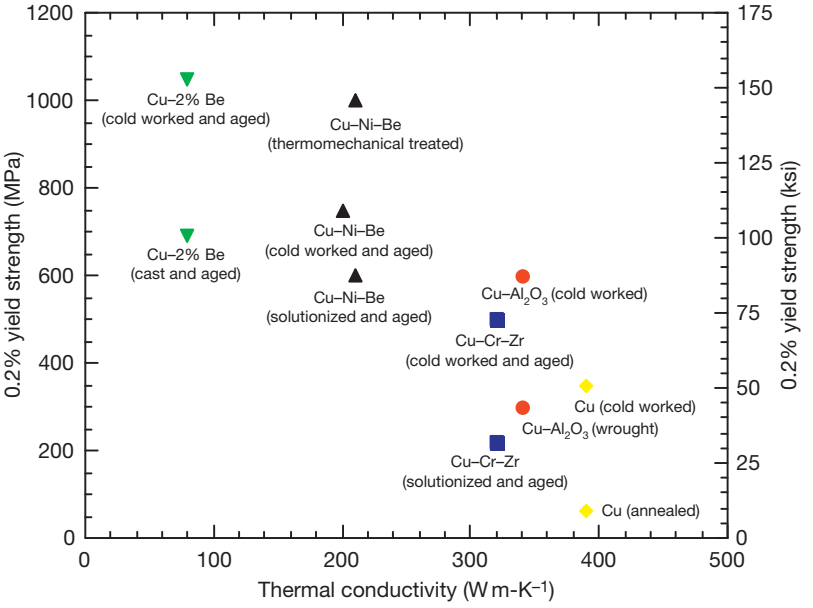

Figure 2 Strength and conductivity of copper and copper alloys. After Li, G.; Thomas, B. G.; Stubbins, J. F. *Metall. Mater. Trans. A* **2000**, *31A*, 2491.

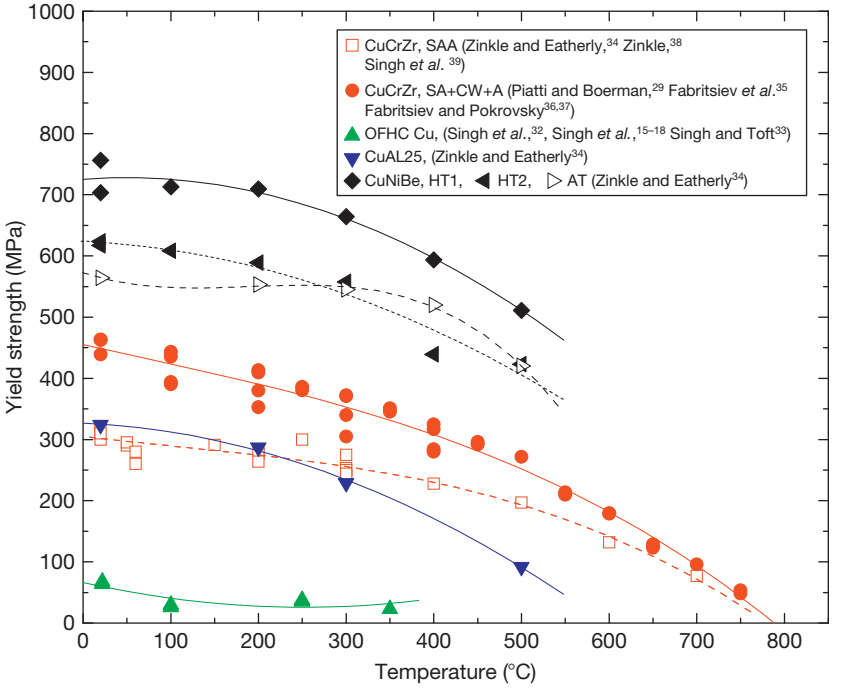

Figure 3 The yield strength of copper alloys as a function of temperature.

the three copper alloys, the CuCrZr alloy has the best ductility over the temperature range, and the ductility of the CuNiBe alloy is the lowest.

Because of the sensitivity of mechanical properties to thermal–mechanical treatments in PH copper alloys, the strength of large components made of these alloys can be significantly lower. For example, during component manufacturing, CuCrZr often experiences additional thermal cycles, such as brazing, welding, or HIPing. While solution annealing

can be conducted during or after a brazing or HIPing process, rapid quenching is not feasible for large components, and a much slower cooling rate (e.g., furnace cooled or gas cooled) is applied in the manufacturing cycle. Significant reduction in strength due to slow cooling rates has been reported in CuCrZr.[30,40–42] A slow cooling rate (50–80 °C min^{-1}) and overaging at 560 °C/2 h significantly reduced the yield stress and the ultimate tensile strength, and tensile elongations of CuCrZr relative to prime-aged CuCrZr.[14] Cooling rates >1200 °C min^{-1} are required to fully quench the Cu–Cr solid solution.[43–45]

The effect of strain rate on tensile properties for pure copper and PH CuCrZr and CuNiBe alloys as well as DS CuAl25 alloy was studied at temperatures of 20 and 300 °C.[14,34,46] All three copper alloys are relatively insensitive to strain rate at room temperature. The strain rate sensitivity parameter of m (where $\sigma_y = C\dot{\varepsilon}^m$ and C is a constant) is ~0.01 for the CuAl25 alloy at room temperature. The strain rate sensitivity of this alloy increases significantly with increasing temperature as reflected by a strain rate sensitivity parameter of $m \sim 0.07$ at 300 °C. Stephens *et al.*[47] reported a strain rate sensitivity parameter of $m \sim 0.1$ in the temperature range of 400–650 °C for CuAl25. A similar effect of strain rate on ultimate tensile strength was also observed on these materials.[34,46] Edwards[46] investigated the strain rate effect of copper alloys in air and vacuum, and found that testing in air or vacuum did not appear to change the strain rate dependence of the CuAl25 alloy, but that testing the CuNiBe alloy in air shifted the embrittlement to a lower temperature.

4.20.4.2 Fracture Toughness

Fracture toughness data for PH copper alloys, CuCrZr and CuNiBe, and DS copper alloys, CuAl15 and CuAl25, are summarized in **Figure 4**.[14,48–50] CuCrZr has the highest toughness, and CuNiBe the lowest among these alloys. The large scatter in measured fracture toughness values for CuCrZr in different studies is likely due to different heat treatments, specimen geometry and dimensions, and testing methods. The temperature dependence of the fracture toughness in CuCrZr, while difficult to accurately define, shows an initial decrease with increasing temperature, and then a slight recovery at temperatures above 250 °C. The effect of thermal–mechanical treatment on fracture toughness of CuCrZr is insignificant in comparison with its effect on tensile properties.[14] The minimum value of the $\mathcal{J}_Q$ for unirradiated CuCrZr is as high as ~100 kJ m^{-2}.

The fracture toughness of DS CuAl15 and CuAl25 is significantly lower than that of CuCrZr, and shows a strong directional dependence. The toughness is higher in the L-T orientation than in the T-L orientation. The fracture toughness decreases

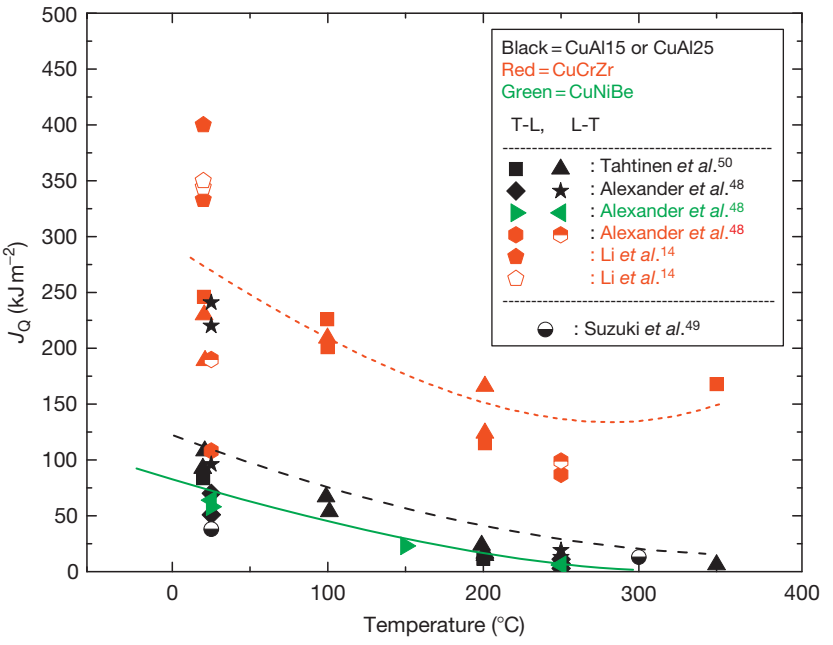

Figure 4 Fracture toughness data of PH CuCrZr, CuNiBe and DS CuAl15, CuAl25.

rapidly with increasing temperature. The $\mathcal{J}_Q$ value for CuAl25 is only $7\,\mathrm{kJ\,m^{-2}}$ at 250 °C in the T-L orientation.[48]

4.20.4.3 Creep

Thermal creep of copper and copper alloys can be significant at relatively low temperatures, because of copper's low melting point ($0.3\,T_m = \sim 134\,^\circ\mathrm{C}$, T_m is the melting point). Nadkarni[51] and Zinkle and Fabritsiev[2] compared the 100-h creep rupture strength of copper and several PH and DS copper alloys at elevated temperatures. Copper alloys have significantly higher creep rupture strength than pure copper. Creep rupture strength decreases drastically as temperature increases in PH alloys such as CuCrZr, as well as in pure copper, between 200 and 450 °C. DS alloys such as CuAl25 have superior creep rupture strength even above 400 °C because of their thermal stability at high temperatures.

Li *et al.*[31] summarized steady-state thermal creep data for pure copper and several copper alloys, as shown in **Figure 5**. Pure copper can suffer significant creep deformation at high temperature even with a very low applied stress. The creep rate of pure copper can be as high as $\sim 10^{-4}\,\mathrm{s^{-1}}$ at ~ 100 MPa at 400 °C. The creep resistance of copper alloys is considerably higher than that of pure copper. The creep rates of copper alloys strongly depend on the applied stress and the temperature, and can be described by the Norton power law relation; that is, $\dot{\varepsilon} = A\sigma^n \exp(-Q/RT)$ where $\dot{\varepsilon}$ is creep rate, σ is the applied stress, n is the stress exponent, Q is the activation energy, R is the gas constant, and T is the temperature. DS copper alloys exhibit unusually high values of the stress exponent, for example, 10–21 in the temperature range of 472–721 °C for GlidCop Al15.[52]

Because of the time-dependent nature of creep deformation, softening behavior due to overaging and recrystallization must be considered during the creep analysis for PH copper alloys. The creep properties of this class of alloys could be significantly changed during prolonged exposure at elevated temperature.

4.20.4.4 Fatigue and Creep–Fatigue

Copper alloys are subjected to severe thermal cycles in high heat flux applications in fusion systems, and so, fatigue as well as creep–fatigue performance is a primary concern. **Figure 6** shows the fatigue performance of OFHC Cu, PH CuCrZr and CuNiBe, and DS CuAl25.[53] All three copper alloys show significantly better fatigue performance than OFHC copper. Among the three alloys, CuNiBe has the best

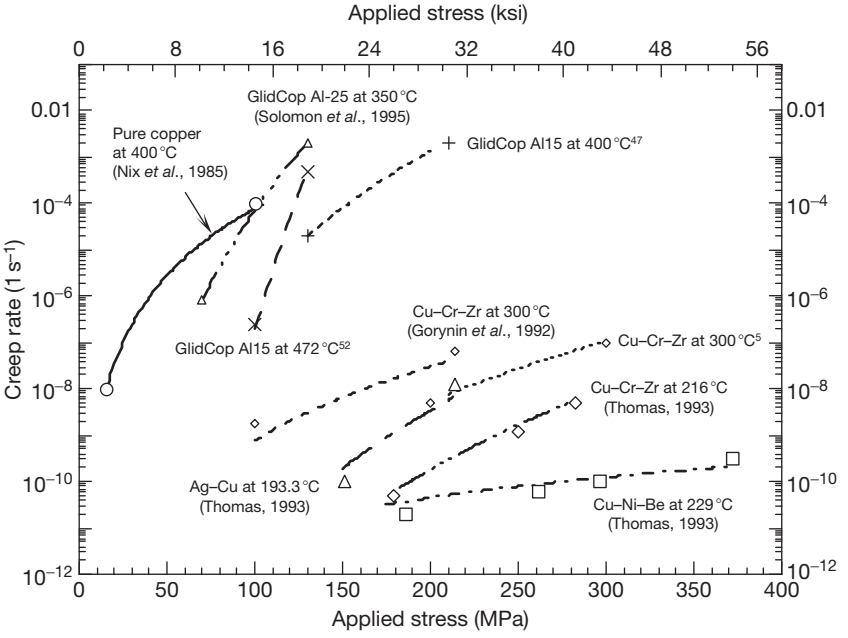

Figure 5 Steady-state thermal creep laws for copper alloys. After Li, G.; Thomas, B. G.; Stubbins, J. F. *Metall. Mater. Trans. A* **2000**, *31A*, 2491.

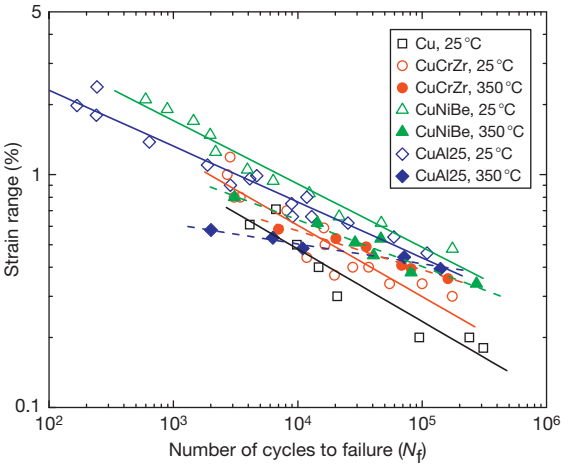

Figure 6 Fatigue performance of OFHC copper, precipitation-hardened CuCrZr and CuNiBe, and dispersion-strengthened CuAl25 in the temperature range of 25–350 °C.

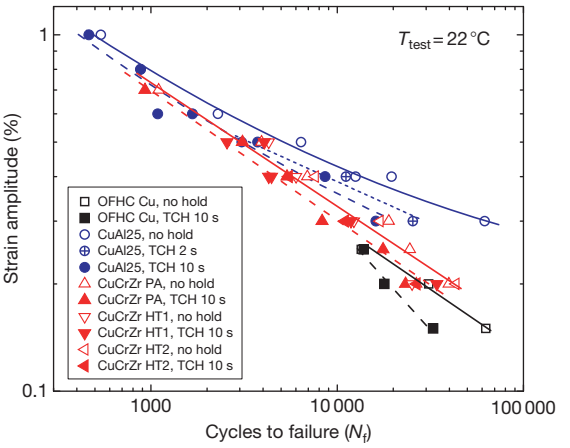

Figure 7 Hold time effect on the fatigue life of OFHC copper, DS CuAl25, and PH CuCrZr with three different heat treatments (prime aged (PA): solution annealed at 1233 K for 3 h, water quenched, and then heat treated at 733 K for 3 h; heat treatment 1 (HT1): PA plus an additional anneal in vacuum at 873 K for 1 h and water quenched; and heat treatment 2 (HT2): PA plus an additional anneal in vacuum at 873 K for 4 h (and water quenched) tested at room temperature. TCH, tension and compression hold.

fatigue response. The temperature dependence of fatigue behavior is stronger in CuAl25 and CuNiBe than in CuCrZr at temperatures between 25 and 350 °C. Heat treatments have an insignificant effect on fatigue life in CuCrZr.[54]

The fatigue life of copper and copper alloys can be significantly reduced when a hold time is applied at peak tensile and/or compressive strains during fatigue cycling. The hold time effect is evident even at room temperature and with a hold time as short as a few seconds.[53,55,56] As shown in **Figure 7**, the fatigue life of OFHC copper is reduced significantly by the introduction of a hold time of 10 s at both tensile and compressive peak strains. The reduction in fatigue life is more severe in the high-cycle, long-life regime than in the low-cycle, short-life fatigue regime. A similar effect of the hold time was observed in copper alloys. The hold time effect appears to be more severe in CuAl25 than in CuCrZr. The effect of hold time is stronger in overaged CuCrZr (e.g., HT2 in **Figure 7**) than in prime-aged CuCrZr. Stress relaxation was observed during the hold periods even at room temperature where thermally activated creep processes are not expected. The reduction in fatigue life is apparently due to a change in the crack initiation mode from transgranular with no hold period to intergranular with a hold period.[56,57] The fatigue life reduction under creep–fatigue loading could be more severe at high temperatures, particularly in PH copper alloys. Their softening behavior at elevated temperature due to overaging and recrystallization could have significant impact on the fatigue life with a very long hold time.

Few studies have been performed to characterize the fatigue propagation rates of copper alloys. The fatigue crack growth rate of CuAl25 was found to be higher than that of CuCrZr at a lower stress intensity range, ΔK, at room temperature.[58] Crack growth rates of CuCrZr and CuAl25 alloys increase with increasing temperature.[49,59]

4.20.5 Irradiation Effects in Copper and Copper Alloys

The irradiation behavior of copper and copper alloys has been extensively studied up to high doses (>100 dpa) for irradiation temperatures of ~400–500 °C.[60] Most of the irradiation experiments of copper and copper alloys have been done in mixed spectrum or fast reactors, such as HFIR, Fast Flux Test Facility (FFTF), or EBR-II. It should be noted that the accumulation rate of helium in copper in fusion reactors is significantly higher than in fission reactors (~10 appm dpa^{-1} in fusion reactors vs. 0.2 appm dpa^{-1} in fast reactors).[22] Attention must be paid to transmutation effects such as helium when the irradiation data of copper and copper alloys from fission reactors are applied for fusion reactor design.

4.20.5.1 Effect of Irradiation on Physical Properties of Copper and Copper Alloys

Neutron irradiation leads to the formation of transmutation products and of irradiation defects, dislocation loops, stacking fault tetrahedra (SFT), and voids. All these features result in reduction of electrical and thermal conductivities.[36,37,61–63] At irradiation temperatures between 80 and 200 °C, the electrical resistivity is controlled by the formation of dislocation loops and stacking fault tetrahedra and transmutation products. The resistivity increase from radiation defects increases linearly with increasing dose up to ~0.1 dpa and saturates. The maximum measured resistivity increase at room temperature is about ~6%. At irradiation temperatures above ~200 °C, the conductivity change from extended radiation defects becomes less significant, and void swelling becomes important to the degradation of the electrical conductivity.

Fusion neutrons produce a significant amount of gaseous and solid transmutation products in copper. The major solid transmutation products include Ni, Zn, and Co. The calculated transmutation rates for copper in fusion first wall at 1 MW-year m^{-2} are 190 appm dpa^{-1} Ni, 90 appm dpa^{-1} Zn, and 7 appm dpa^{-1} Co.[2] Ni is the main transmutation element that affects the thermal conductivity of copper. It should be noted that water-cooled fission reactors would produce significantly higher transmutation rates of copper to Ni and Zn (up to ~5000 and 2000 appm dpa^{-1}, respectively) because of thermal neutron reactions. The data from fission reactor irradiation experiments must be treated with care when they are applied for fusion design.

4.20.5.2 Effect of Irradiation on Mechanical Properties of Copper and Copper Alloys

4.20.5.2.1 Tensile properties

Irradiation causes large changes in tensile properties of copper and copper alloys. Copper and copper alloys can be hardened or softened by irradiation, depending on the irradiation temperature and the amount of the cold work prior to irradiation. Irradiation hardening of copper and copper alloys due to defect cluster formation is significant at irradiation temperatures <300 °C. Irradiation softening occurs at irradiation temperatures >300 °C because of radiation-enhanced recrystallization and precipitate coarsening in PH copper alloys.

Low-temperature neutron irradiation of pure copper leads to development of a yield drop and significant hardening. Typical stress–strain behavior of pure copper and copper alloys irradiated to low doses at low temperatures is illustrated in **Figure 8**. The data of irradiated copper are from the work of Edwards *et al.*,[64] and the data of irradiated CuCrZr from Li *et al.*[14] Irradiation significantly changes the work hardening behavior of pure copper. Work hardening capability is progressively reduced with increasing doses. Appreciable work hardening still exists at the dose of 0.1 dpa. The effect of irradiation on the tensile behavior of copper alloys can be quite different. A complete loss of work hardening capability and

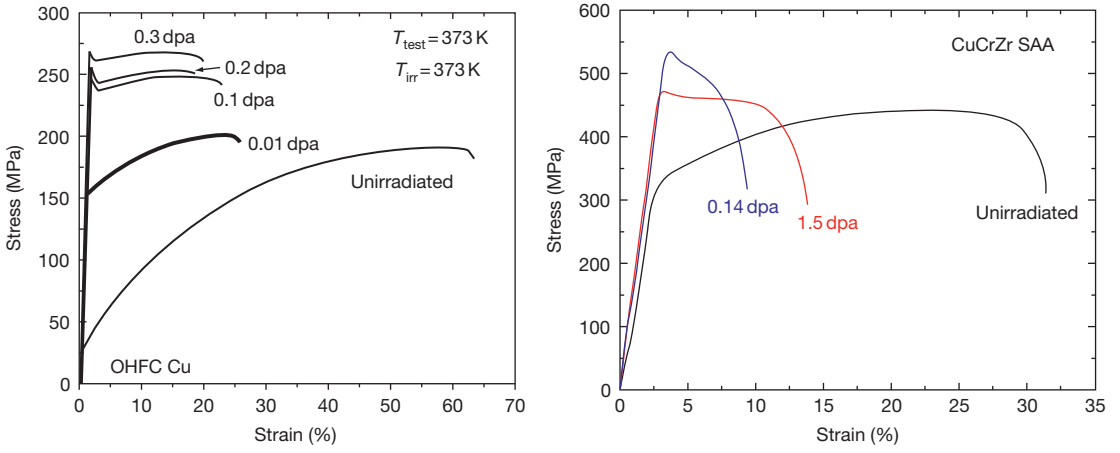

Figure 8 Engineering stress–strain curves for OFHC copper (left) neutron irradiated at 100 °C and for precipitation-hardened CuCrZr (right) neutron irradiated at 80 °C. The plot for copper is from the reference. Reproduced from Edwards, D. J.; Singh, B. N.; Bilde-Sørensen, J. B. *J. Nucl. Mater.* **2005**, *342*, 164.

uniform elongation occurs at 0.14 dpa in neutron-irradiated CuCrZr in the prime-aged condition. Irradiation to 1.5 dpa further reduces the yield strength, and recovers some total elongation in CuCrZr.

The dose dependence of radiation hardening in copper at irradiation temperatures of 30–200 °C is summarized by Zinkle *et al.*, and shown in Figure 9.[65,66] Radiation hardening in copper can be observed at a dose as low as 0.0001 dpa. The yield stress increases dramatically with increasing dose and saturates at ~0.1 dpa. Significant radiation hardening is accompanied by loss of strain hardening capabilities, resulting in prompt necking upon yielding.

The temperature dependence of radiation hardening of pure copper at different irradiation temperatures was summarized and discussed by Fabritsiev and Pokrovsky.[67] The radiation hardening decreases with increasing irradiation temperature in copper. The magnitude of radiation hardening is ~200 MPa at 80 °C, while only ~40 MPa at 300 °C at a dose of 0.1 dpa. Annealing at temperatures higher than 0.4 T_m can effectively reduce the defect cluster density in copper. Annealing at 300 °C for 50 h after irradiation of copper to 0.01–0.3 dpa at 100 °C and annealing at 350 °C for 10 h after irradiation of CuCrZr IG and GlidCop Al25 IG to 0.4 dpa at 150 °C can essentially recover the ductility of the copper and copper alloys.[68,69] However, postirradiation annealing also reduces the critical stress for flow localization in pure copper.[70]

Irradiation creates a large increase in strength and decrease in ductility in copper alloys for irradiation temperatures below 300 °C. The strengthening effect decreases with increasing temperature. The crossover to radiation softening occurs at approximately 300 °C. The radiation softening effect in CuAl25 alloy is not as strong as for CuCrZr alloy where precipitate stability may be an issue. Neutron-irradiated copper alloys exhibit low uniform elongation after low-dose, low-temperature irradiation. The uniform elongation is recovered to near unirradiated values at 300 °C. Figure 10 compiles the yield strength data for PH CuCrZr and DS copper alloys (CuAl 25, CuAl15, MAGT 0.2) as a function of dose for the irradiation temperature of ~100 °C.[14,71] Both alloys show significant radiation hardening at low doses and an apparent saturation at ~0.1 dpa. Irradiation-induced hardening is accompanied by the loss of strain hardening capability and a complete loss of uniform elongation, while the total elongation remains on the level of ~10% for doses up to 2.5 dpa for CuCrZr.

The strain rate dependence of tensile properties in neutron-irradiated CuCrZr was investigated at room temperature by Li *et al.*[14] The strain rate sensitivity is small at room temperature in unirradiated CuCrZr. The measured strain rate sensitivity parameter, m, is <0.01 for CuCrZr. The strain rate sensitivity parameter increased to ~0.02 in CuCrZr after neutron irradiation to 1.5 dpa. Zinkle *et al.*[65] observed a small strain rate dependence of tensile strength in GlidCop Al15 and MAGT 0.2 neutron irradiated to ~13 dpa at 200 °C with $m \sim 0.02$ for GlidCop

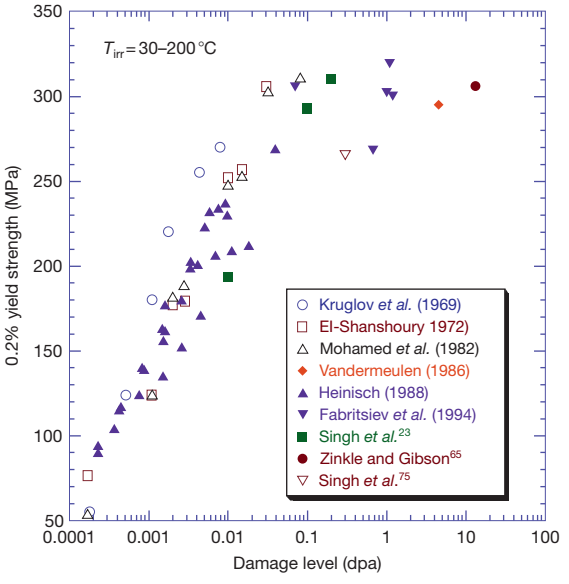

Figure 9 Radiation hardening in copper. Reproduced from Zinkle, S. J.; Gibson, L. T. *Fusion Materials Semi-annual Progress Report*; DOE/ER-0313/27; Oak Ridge National Laboratory, 1999; p 163.

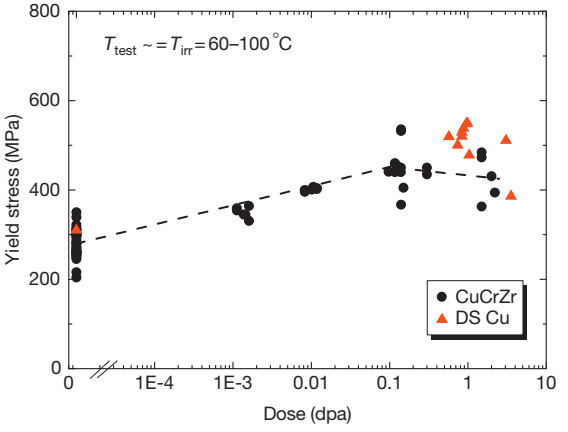

Figure 10 Dose dependence of the yield strength in CuCrZr and DS copper alloys irradiated at low temperatures.

Al15 and $m < 0.01$ for MAGT 0.2. In general, the strain rate and temperature dependence of flow stresses is small in fcc metals.

4.20.5.2.2 Fracture toughness

Fracture toughness data for irradiated copper alloys are scarce. The effect of neutron irradiation on fracture toughness has been studied in two alloys, CuCrZr and CuAl25.[14,50,72] Fracture toughness data on neutron-irradiated CuAl25 are available to a dose of 0.3 dpa, and for CuCrZr, the data are available up to 1.5 dpa (Figure 11). Neutron irradiation to 0.3 dpa significantly reduced the fracture toughness of CuAl25 in the temperature range of 20–350 °C. The toughness of irradiated CuAl25 is two to three times lower than that of the unirradiated alloy. The effect of neutron irradiation on fracture toughness of CuCrZr was less pronounced, despite the significant effect on the tensile properties even at relatively low doses (0.14–0.15 dpa). Reduction of fracture toughness in irradiated CuCrZr was small, and the $\mathcal{J}_Q$ value was still >200 kJ m^{-2} up to 1.5 dpa (Figure 11).[14]

4.20.5.2.3 Fatigue and creep–fatigue

The effect of irradiation on fatigue performance has been evaluated for PH CuCrZr and DS CuAl25.[73] The fatigue data for unirradiated and irradiated CuAl25 and CuCrZr in the temperature range of 20–350 °C are compiled and compared in Figure 12.[24,53,74–76] The effect of irradiation on the fatigue response of CuAl25 is small at low temperature. However, the fatigue life is reduced significantly at 250 and 350 °C because of radiation exposure. The fatigue life of the CuCrZr alloy was reduced following irradiation at 250 and 350 °C, similar to CuAl25. The degradation in the fatigue performance of these two alloys from irradiation exposure was not as severe as that in the tensile properties.

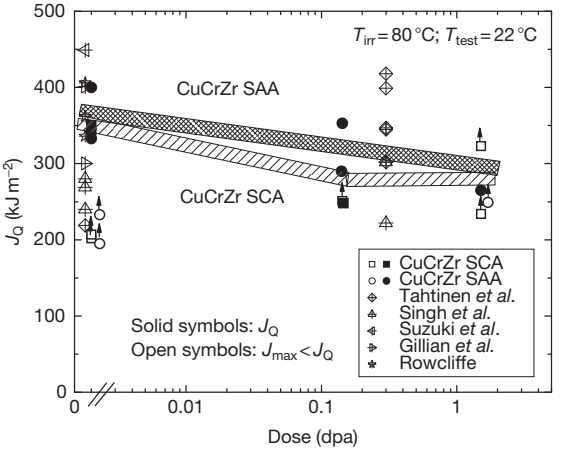

Figure 11 Fracture toughness of CuCrZr with two heat treatments as a function of dose. The heat treatment, SCA, was to simulate the manufacturing cycle for ITER large components. Reproduced from Li, M.; Sokolov, M. A.; Zinkle, S. J. *J. Nucl. Mater.* **2009**, *393*, 36.

Creep–fatigue behavior of neutron-irradiated CuCrZr was investigated at a dose level of 0.2–0.3 dpa at 22 and 300 °C by Singh *et al.*[54] Hold times of 10 and 100 s were applied during fatigue cycling. Radiation hardening at low temperatures (e.g., 60 °C) is beneficial to the fatigue performance, while irradiation at high temperatures (e.g., 300 °C) has no significant effect on the creep–fatigue life of irradiated CuCrZr. A number of in-reactor creep–fatigue experiments were performed on a CuCrZr alloy in the BR-2 reactor at Mol (Belgium) by Singh *et al.*[77] The irradiation experiments were carried out at 70 and 90 °C at the strain amplitude of 0.5% with hold times of 10 and 100 s. The key finding was that neither the irradiation nor the hold time has any significant effect on the fatigue life of CuCrZr during the in-reactor tests.

4.20.5.2.4 Irradiation creep and void swelling

There is limited literature on irradiation creep of copper and copper alloys.[78–82] A study by Witzig[82] showed no enhancement of creep rates in copper relative to thermal creep at 260 °C and 69 MPa under light ion irradiation. Jung[79] studied irradiation creep of 20% cold-worked copper foils at temperatures of 100–200 °C and the applied tensile stress of 20–70 MPa under 6.2 MeV proton irradiation with displacement rates of $0.7–3.5 \times 10^{-6}$ dpa s^{-1}. The irradiation creep rate showed a linear stress dependence with the irradiation creep compliance of 6.2×10^{-11} Pa^{-1} dpa^{-1} at stresses <50 MPa at 150 °C, comparable to that of other fcc metals such as Ni and austenitic stainless steels. At higher stresses (>50 MPa), the creep rate showed a power law relation with the stress exponent of 4. Ibragimov *et al.*[78] investigated in-reactor creep of copper in the WWR-K water-cooled reactor at a neutron flux of 2.5×10^{15} m^{-2} s^{-1} ($E > 0.1$ MeV) at 150–500 °C and 20–65 MPa. The in-reactor creep rate of copper was significantly higher than the thermal creep rate at temperatures below 0.4 T_m (T_m is the melting point). The stress dependence of the in-reactor creep rate showed a power law relation with the stress exponent of ~3.

Pokrovsky *et al.*[80] reported irradiation creep data for DS MAGT 0.2. The irradiation creep experiments were performed using pressurized tubes

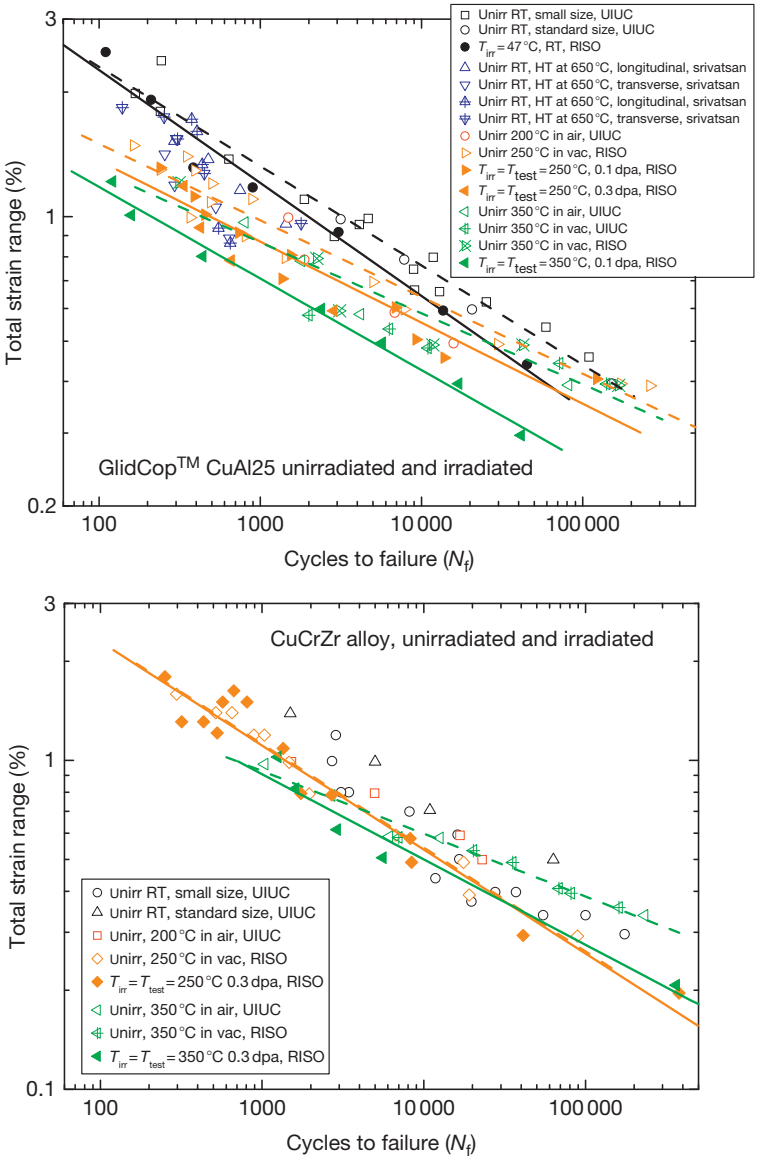

Figure 12 Effect of irradiation on fatigue life of CuAl25 (top) and CuCrZr (bottom) between room temperature and 350 °C.

irradiated in coolant water in the core position of the SM-2 reactor to ~3–5 dpa at temperatures of 60–90 °C. A creep rate as high as $\sim 2 \times 10^{-9}\,s^{-1}$ was observed at a hoop stress of 117 MPa.

Radiation-induced void swelling in copper and copper alloys has been studied extensively. Zinkle and Farrell[83,84] measured the temperature-dependence of void swelling in pure copper and a dilute Cu–B alloy neutron irradiated to ~1.1–1.3 dpa at a damage rate of 2×10^{-7} dpa s^{-1} at temperatures of 180–500 °C (**Figure 13**). Maximum swelling occurs at ~300–325 °C in pure copper under fission neutron irradiation conditions. The lower temperature limit for void swelling is ~180 °C, and the higher temperature limit ~500 °C. Low-dose irradiation (<0.2 dpa) often leads to inhomogeneous void formation and nonlinear swelling behavior.[60] A steady-state swelling rate of ~0.5%/dpa is observed in copper at high doses, and the swelling level can be as high as 60%.[60,85] Variations in displacement damage rate can shift the peak swelling temperature. An order of magnitude decrease in neutron flux can lower the peak swelling temperature by ~20 °C. The peak swelling temperature shift can be as high as ~165 °C between neutron irradiation (10^{-7} dpa s^{-1}) and ion irradiation (10^{-3} dpa s^{-1}).

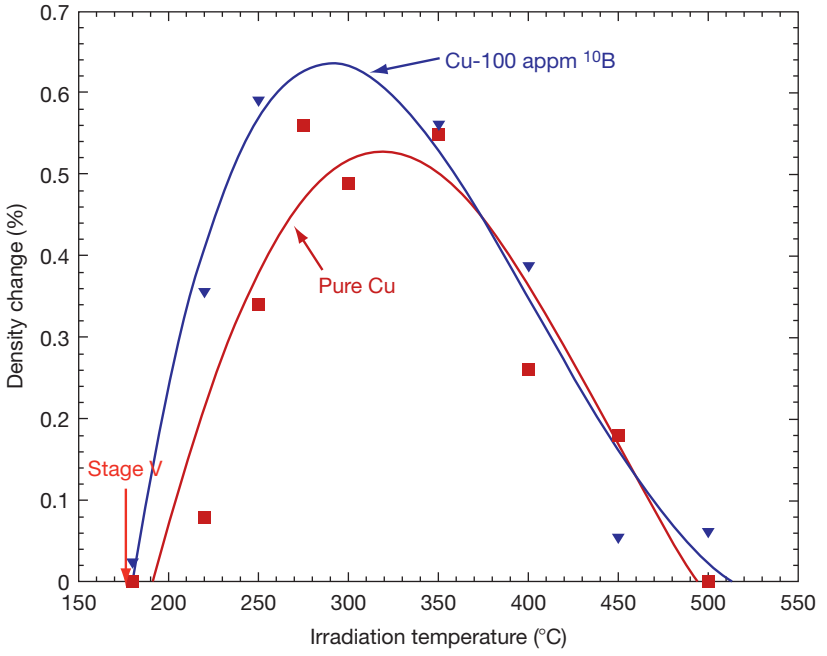

Figure 13 Swelling in pure copper and Cu–B alloy. Reproduced from Zinkle, S. J.; Farrell, K. *J. Nucl. Mater.* **1989**, *168*, 262; Zinkle, S. J.; Farrell, K.; Kanazawa, H. *J. Nucl. Mater.* **1991**, *179–181*, 994.

Residual impurity oxygen can have a significant effect on void swelling in copper. A number of neutron, ion, and electron irradiation studies have shown that voids are not formed in high-purity, low-oxygen copper over the wide range of irradiation temperatures.[60,86] The oxygen content should be maintained below ~10 wt ppm to minimize void swelling in copper.

The effect of helium production on void formation and swelling in copper is a significant concern for its fusion applications.[87] Helium effects have been studied by either dual-beam ion irradiation[88,89] or neutron irradiation of Cu–B alloys.[89] Significant enhancement of void formation and swelling was observed in copper under ion irradiation with simultaneous helium implantation. Neutron irradiation of copper containing ~18 wppm ^{10}B to ~1.2 dpa for the irradiation temperatures of 182–500 °C showed that the peak swelling temperature and the lower swelling temperature limit shifted to lower values (**Figure 13**). A recent study by Xu *et al.*[90] of materials enriched in the copper isotopes, ^{63}Cu, $^{63+65}$Cu, and ^{65}Cu neutron irradiated in the Materials Open Test Assembly (MOTA) in the FFTF at irradiation temperatures of 373–410 °C to doses up to 15.4 dpa found that both H and He enhanced void swelling in copper. The H effect is important at lower temperatures when the H production is considerably higher than the He production. At 410 °C the hydrogen effect decreases dramatically and void swelling is affected by the helium concentration.

PH and DS copper alloys have superior void swelling resistance compared to pure copper under fission neutron irradiation.[2,71] Both PH CuCrZr and DS CuAl25 showed <2% swelling after irradiation to 150 dpa at ~415 °C.[85,91] When irradiated to 98 dpa at 450 °C, only ~2% swelling was observed in CuAl25. The CuAl25 alloy appears to have the best resistance to void swelling among the copper alloys.[92] However, the swelling resistance of DS copper alloys can be significantly reduced when there is a high generation rate of helium. While CuAl25 showed negligible swelling after irradiation to 103 dpa at 415 °C in the FFTF, boron-doped CuAl15 showed 11% swelling under the same irradiation condition.[93] Fabritsiev *et al.*[22] reported a swelling rate of 1%/dpa for CuAl25 + B alloy even at a low dose of ~0.5 dpa at 300 °C, because of high helium accumulation. The boron-free MAGT 0.2 alloy did not show swelling in the same experiment. Simultaneous heavy ion irradiation and helium implantation in GlidCop Al60 at 350 °C showed an increase of the swelling rate from 0.01%/dpa (single-beam irradiation) to 0.05%/dpa (dual-beam irradiation).[94]

The initial thermal–mechanical treatment of PH copper alloys can have a significant impact on their

swelling resistance. CuNiBe in the cold-worked and aged condition showed ~28% swelling, while CuNiBe in the annealed and aged condition swelled only ~13% after fission neutron irradiation to 98 dpa at 450 °C.[95] The susceptibility to radiation-enhanced recrystallization is more severe in a cold-worked alloy, leading to the swelling instability.

4.20.5.3 Effect of Irradiation on Microstructure of Copper and Copper Alloys

4.20.5.3.1 Defect structure in irradiated copper and copper alloys

Copper is among the most extensively studied metals in terms of fundamental radiation damage. Several reviews on the effect of irradiation on the microstructure of copper and copper alloys are available in the literature.[60,96,97] Neutron irradiation of copper at low temperatures produces small defect clusters, dislocation loops, and SFTs. At temperatures above ~150–180 °C, the density of defect clusters starts to decrease with increasing temperature, accompanied by the formation of voids. This temperature-dependent formation of defect structures is shown in **Figure 14**.[60] Low-temperature neutron irradiation produces a high number density of SFTs and a low number density of dislocation loops in copper. Edwards *et al.*[64] reported a number density of SFTs, $\sim 2\text{–}4 \times 10^{23}\ \mathrm{m}^{-3}$ and a number density of dislocation loops, $5 \times 10^{21}\ \mathrm{m}^{-3}$ in OFHC copper neutron irradiated to ~0.01 dpa at 100 °C. Dislocation loops are believed to be of interstitial type.

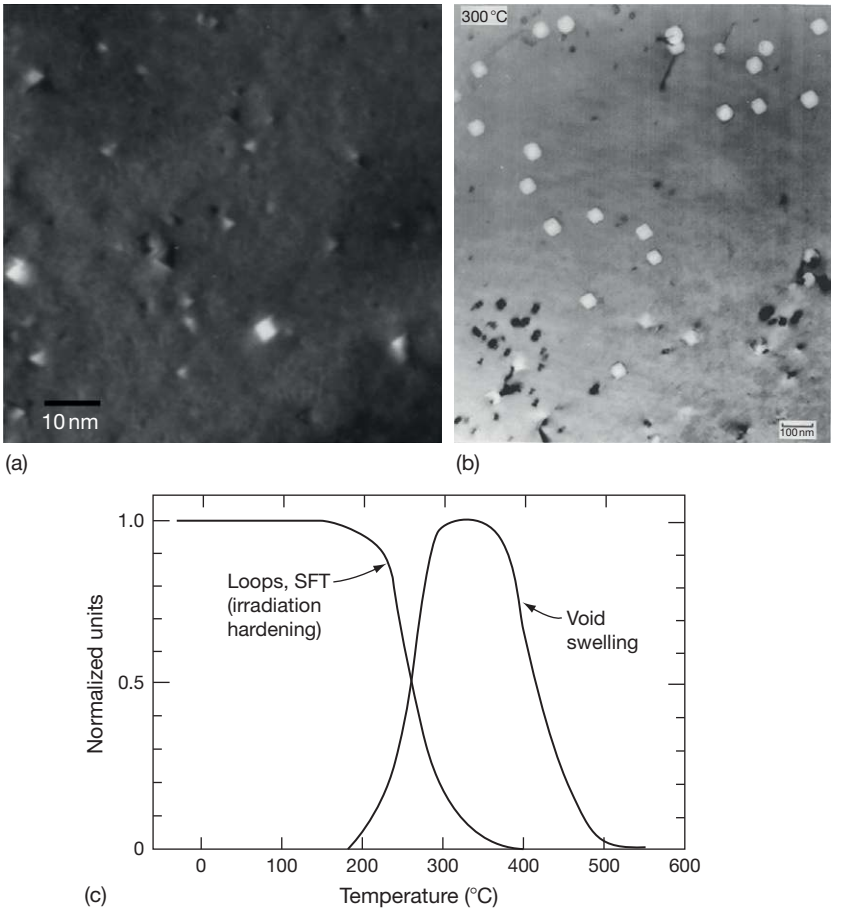

Figure 14 (a) Stacking fault tetrahedra and defect clusters produced in OFHC copper during irradiation to 1.9 dpa at 180 °C (reproduced from Zinkle, S. J.; Matsukawa, Y. *J. Nucl. Mater.* **2004**, *329–333*, 88), (b) voids in copper irradiated at 300 °C (reproduced from Zinkle, S. J.; Farrell, K. *J. Nucl. Mater.* **1989**, *168*, 262). (c) Schematic drawing showing the temperature dependence of defect cluster formation and void swelling (reproduced from Zinkle, S. J. In *Effects of Radiation on Materials*, ASTM STF 1125, 15th International Symposium); Stoller, R. E., *et al.*, Eds.; American Society for Testing and Materials: Philadelphia, 1992; p 813.

The size of SFTs is small, ~2–3 nm. As doses increased, the density of SFTs increased to a saturation level at ~0.1 dpa, while the size of SFT is independent of the dose and temperature. In general, the dislocation loop density is low, and a significant dislocation network is not formed in irradiated copper.[96]

Radiation hardening in copper can be adequately described by Seeger's dispersed barrier model, and the yield strength increase is due to the formation of defect clusters.[98] Singh and Zinkle[96] summarized the dose dependence of the TEM-visible defect cluster density in copper irradiated near room temperature with fission neutrons, 14 MeV neutrons, spallation neutrons, and 800 MeV protons (**Figure 15**)[96] TEM-visible defect clusters were observed at a very low dose (10^{-5} dpa). The defect cluster density showed a linear dependence on irradiation dose at low doses. The dose dependence of the defect cluster density shifts to either a linear or a square root relation at intermediate doses (>~0.0002 dpa). The cluster density reaches an apparent saturation ($\sim 1 \times 10^{24}\,m^{-3}$) at ~0.1 dpa. The dislocation loops range in size from ~1 to 25 nm.[99] Differences in the type of irradiation (fission, fusion, spallation, etc.) have no significant effect on the defect cluster accumulation behavior in copper. The density of defect clusters in irradiated copper shows strong temperature dependence (**Figure 16**).[100] The defect cluster density is essentially independent of the irradiation temperature between 20 and 180 °C (upper temperature limit is dependent on dose rate). At higher temperature, the cluster density decreases rapidly with increasing irradiation temperature. At irradiation temperatures between 182 and 450 °C, the density of defect clusters was reduced by over three orders of magnitude.[83,84] The saturation dose of the defect cluster density is similar, ~0.1 dpa, for all irradiation temperatures.[96] The size distribution of visible defect clusters can be described by an exponential function[101]: $N(d) = N_0 \exp(-d/d_0)$, where $N(d)$ is the number of defects of diameter d, N_0, and d_0 are constants, and their values depend on irradiation conditions and material purity. As the irradiation temperature decreases, a fraction of small clusters increases relative to large clusters.

Void formation occurs above ~180 °C in neutron-irradiated copper.[60] The peak void swelling temperature in copper is about 320 °C at a dose rate of $2 \times 10^{-7}\,dpa\,s^{-1}$. Singh and Zinkle[96] summarized the dose dependence of void density measured by TEM in copper irradiated with fission and fusion neutrons at 250–300 °C from several studies. The data showed a large variation (up to two orders of magnitude differences) of void density between

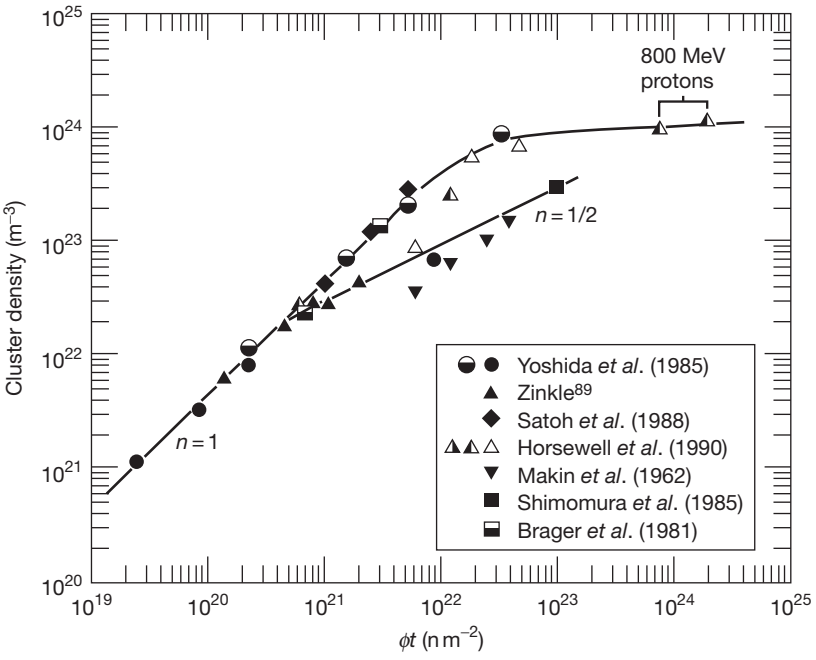

Figure 15 Dose dependence of defect cluster density in copper irradiated near room temperature. Reproduced from Singh, B. N.; Zinkle, S. J. *J. Nucl. Mater.* **1993**, *206*, 212.

experiments. One possible source could be residual gas atoms in copper that can have a dramatic effect on void swelling in copper. Zinkle and Lee[86] discussed in detail the effect of oxygen and helium on the formation of voids in copper. The stacking fault tetrahedron is predicted to be the most stable configuration of vacancy clusters in copper. A small amount of oxygen (~10 appm) or helium (~1 appm) in copper is needed to stabilize voids. High-purity copper with low oxygen concentration (<5 wppm) showed no significant void formation after 14 MeV Cu ion irradiation to 40 dpa at temperatures of 100–500 °C.[100]

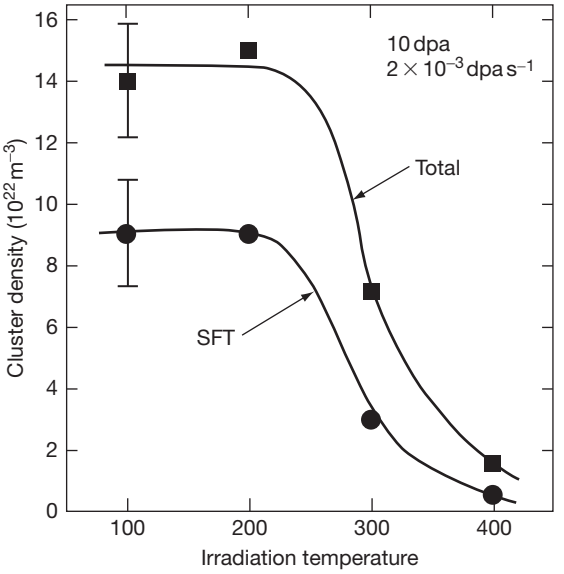

Figure 16 Measured defect cluster density in 14-MeV Cu^{3+} ion-irradiated copper as a function of irradiation temperature. Reproduced from Zinkle, S. J.; Kulcinski, G. L.; Knoll, R. W. *J. Nucl. Mater.* **1986**, *138*, 46.

The defect microstructure (SFTs and dislocation loops) in irradiated copper alloys is essentially the same as in irradiated pure copper.[22,25,64] Neutron irradiation can affect precipitate microstructure in copper alloys. When irradiated at 100 °C, the precipitate density in CuCrZr was slightly reduced, and the mean size of the precipitates increased.[13,64] Zinkle *et al.*[25,26] reported that when GlidCop Al25 and MAGT 0.2 were ion irradiated to 30 dpa at 180 °C, a high number density (5×10^{23} m^{-3}) of defect clusters (primarily SFTs) with a mean size of 2 nm was produced. The geometry of oxide particles in GlidCop Al25 was transformed from triangular platelets to nearly circular platelets, and the particle size was reduced from 10 to 6 nm after irradiation (**Figure 17**).[25,26] The geometry and size of oxide particles in MAGT 0.2 were essentially unchanged by irradiation. In general, DS copper alloys showed superior particle stability under irradiation.

Limited data are available in terms of the effect of solution additions on the irradiated microstructure of copper. A study by Zinkle[25] showed that solute additions (e.g., Al, Mn, Ni) to 5 at% in copper do not have significant effect on the total density of small defect clusters at low irradiation temperatures (≤130 °C). However, solute additions reduce the formation of SFTs and enhance the formation of dislocation loops. The loop density and mean size in Cu–5% Mn irradiated to 1.6 dpa at 160 °C were 3×10^{21} m^{-3} and 23 nm, and 1.8×10^{22} m^{-3} and 18 nm in Cu–5% Ni irradiated to 0.7 dpa at 90 °C

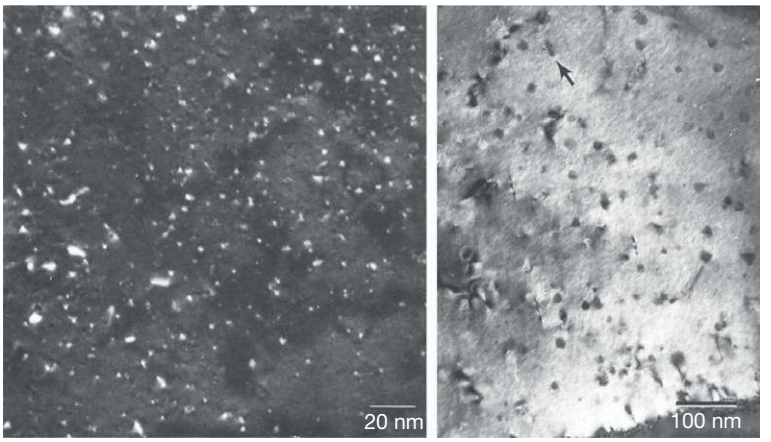

Figure 17 Defect structure (left) and Al_2O_3 particle morphology (right) in 50% cold-worked GlidCop Al25 irradiated with 3 MeV Ar^+ ions to 30 dpa at 180 °C. Reproduced from Zinkle, S. J.; Horsewell, A.; Singh, B. N.; Sommer, W. F. *J. Nucl. Mater.* **1994**, *212-215*, 132; Zinkle S. J.; Nesterova, E. V.; Barabash, V. R.; Rybin, V. V.; Naberenkov, A. V. *J. Nucl. Mater.* **1994**, *208*, 119.

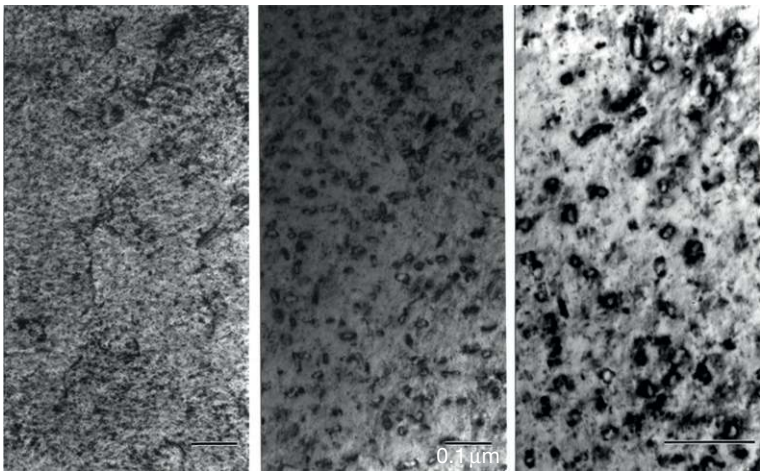

Figure 18 Comparison of the dislocation loop microstructure in irradiated pure copper (left), Cu–5% Mn (center) and Cu–5% Ni (right) alloys. The irradiation conditions were 0.7 dpa at 90 °C (Cu), 1.6 dpa at 160 °C (Cu–5% Mn), and 0.7 dpa at 90 °C (Cu–5%Ni). Reproduced from Zinkle, S. J.; Horsewell, A.; Singh, B. N.; Sommer, W. F. *J. Nucl. Mater.* **1994**, *212-215,* 132; Zinkle S. J.; Nesterova, E. V.; Barabash, V. R.; Rybin, V. V.; Naberenkov, A. V. *J. Nucl. Mater.* **1994**, *208*, 119.

(Figure 18).[25,26] These loop densities are more than an order of magnitude larger than the highest loop density observed in pure copper. The effect of the stacking fault energy on void formation in copper alloys was also investigated. Generally speaking, the lower the stacking fault energy, the less favorable for the formation of 3D voids. For example, swelling occurred in Cu–1–2.5% Ge alloys irradiated at 250 °C, while no measurable swelling occurred in Cu–3–5% Ge that has lower stacking fault energies.[97]

4.20.5.3.2 Dislocation channeling

Dislocation channels are frequently observed during postirradiation deformation of copper and copper alloys.[102,103] Greenfield and Wilsdorf[104] were the first who observed an area free of irradiation defects in the middle of a slip-line cluster by TEM in a neutron-irradiated copper single crystal. Extensive studies were conducted to establish the correlation between the deformation behavior and the slip-line structure in neutron-irradiated copper single crystals.[104–107] Sharp[108–110] studied the deformation and dislocation channels in neutron-irradiated copper single crystals in detail, and established a direct correlation between the surface slip steps and dislocation channels. The channels are nearly free of irradiation-produced defects, and operate parallel to the primary {111} slip plane. The cleared channels are formed by cooperative localized motion of glide dislocations that interact with and annihilate the preexisting radiation defect clusters. The channel characteristics have strong dependence on irradiation dose and test temperatures. The channel width decreases and the slip step height increases with increasing irradiation dose, and the channel width and the slip step height decrease with decreasing deformation temperature. Howe[111] confirmed that the channel width, spacing, the slip step height, and the average shear per slip band increase with increasing test temperature in the temperature range of 4–473 K. The reduction in channel width was considered to be a consequence of impeded cross-slip.[108,111]

Dislocation channels were also observed in neutron-irradiated copper single crystals under cyclic straining.[112,113] The width and average spacing of channels changed with the number of cycles, in contrast to channels formed during tensile straining where the width and spacing of channels were constant over a large range of strains.[108]

Dislocation channels are formed in neutron-irradiated copper alloys as well. Sharp[114] observed the channeling effect in three different copper alloys neutron irradiated at ambient temperature, that is, Cu–0.8% Co, Cu–Al_2O_3, and Cu–4% Al single crystals. The channel spacing in the copper alloys were 1.2–1.5 μm, about half that observed in neutron-irradiated copper single crystals (2.3 μm). The channel width in Cu–0.8% Co alloy is similar to that for irradiated copper crystal (0.16 μm), and the channels have the uniform width along the length. The presence of the second-phase particles in Cu–0.8% Co alloy has little effect on channeling. In the DS Cu–Al_2O_3 alloy, the channels are wider (0.24 μm) and

more irregular in width. The channel width can vary by a factor of 2 within a few microns along the length of a channel. A high density of dislocations surrounding the particles within the channel was observed in Cu–Al_2O_3, indicating great difficulty of dislocations in bypassing the (nondeforming) second-phase particles. In the single-phase Cu–4% Al alloy, however, no dislocation channels were observed.

Edwards[13,40,64,115] studied thoroughly the deformed microstructure in neutron-irradiated CuCrZr alloys, and compared with the deformation microstructure in neutron-irradiated OFHC-Cu (**Figure 19**). Dislocation channels were observed during postirradiation deformation of the CuCrZr alloy neutron irradiated to 0.2–0.3 dpa at 100 °C. Channels were formed even before the upper yield point, and continued throughout the tensile deformation process. Some channels are completely free of defect clusters, and others contain a sizeable population of defect clusters. The width of cleared channels varied between about 100 and 250 nm. The channel formation is more pronounced in a higher-dose specimen than in a lower-dose specimen. In comparison with OFHC-Cu, CuCrZr showed little difference in deformation mode and channel characteristics in terms of width and size. While the channels in the OFHC-Cu were free of defects and dislocation debris, the channels in the CuCrZr alloy contained a small fraction of defects and precipitates. When the irradiated CuCrZr was annealed and deformed, deformation occurs in a much more homogeneous fashion, and no well-defined channels were observed.

The formation of dislocation channels in pure copper was investigated by *in situ* straining experiments on ion-irradiated copper in an electron microscope.[116,117] Postirradiation straining of the thin foils of polycrystalline copper irradiated with 200 keV Kr ions to about 2×10^{-4} to 0.02 dpa at room temperature showed that defect-free channels nucleate at grain boundaries, or in the vicinity of cracks, suggesting that grain boundaries and crack tips are nucleation sites for channels.[117] Cross-slips were found to be responsible for channel widening and defect removal within the channel. Edwards *et al.*[64] studied the initiation and propagation of dislocation channels in neutron-irradiated OFHC-Cu (**Figure 20**) and CuCrZr alloy in an interrupted tensile test. TEM observations suggested that channels are initiated at boundaries, large inclusions, or existing channels. Channels are formed by interactions of newly formed dislocations with irradiation defects on the glide plane. Once formed, the channels propagate rapidly in the grain interior until they intercept another boundary, interface, or channel. Despite significant efforts, the exact mechanism of channel formation and evolution still remains unresolved, and a clear connection between the slip processes, dislocation channeling, and localized flow in neutron-irradiated metals is still lacking.

4.20.6 Joining

Copper and copper alloys can be joined by a variety of techniques, including mechanical coupling, welding, brazing, and diffusion bonding. A comprehensive overview of joining techniques for copper and copper alloys can be found in the reference.[118] The welding techniques commonly used for copper and copper alloys include arc welding, resistance welding, oxy-fuel welding, and electron beam welding. Welding is generally not recommended for joining high-strength copper alloys. PH copper alloys lose their mechanical strength because of the dissolution of precipitates

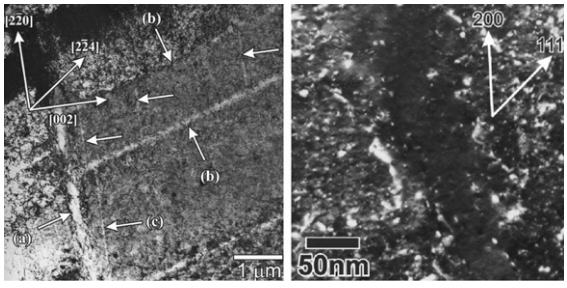

Figure 19 Dislocation channels observed in OFHC-Cu (left) and CuCrZr (right) irradiated to 0.3 dpa at 100 °C. Edwards, D. J.; Singh, B. N.; Xu, Q.; Toft, P. *J. Nucl. Mater.* **2002**, *307–311*, 439; Edwards, D. J.; Singh, B. N.; Bilde-Sørensen, J. B. *J. Nucl. Mater.* **2005**, *342*, 164.

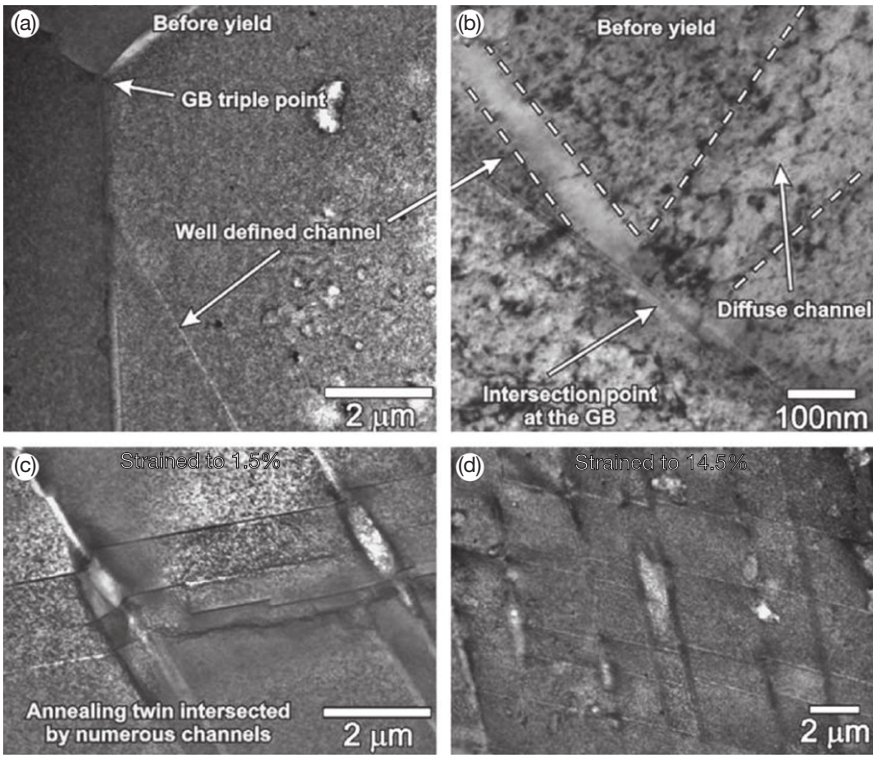

Figure 20 Examples of cleared channels formed in the OFHC-Cu irradiated (to 0.3 dpa) and tested at 323 K to different strain levels: (a) before yield, (b) before yield, (c) 1.5%, and (d) 14.5%. Note that at 14.5% strain level the grain is subdivided by numerous channels formed on different slip planes. All images shown in this figure were taken in the STEM bright field mode. Reproduced from Edwards, D. J.; Singh, B. N.; Bilde-Sørensen, J. B. *J. Nucl. Mater.* **2005**, *342*, 164.

during the welding process. The welded component must be resolution annealed and aged to recover some of the initial strength in the joint. Recrystallization in the melt layer degrades the mechanical property of the weldment. DS copper alloys cannot be welded by conventional welding processes because of the loss of oxide particles and recrystallization in the weld zone.

Brazing is the most common method for joining copper alloys. All conventional brazing techniques can be used to join copper and copper alloys, including furnace brazing, torch brazing, induction brazing, resistance brazing, and dip brazing. A wide range of filler metals are available, and the most common brazing filler metals are Cu–Zn, Cu–P, Cu–Ag–P, and Ag- and Au-based alloys.[118] Ag- and Au-based filler metals are unacceptable in fusion reactor environments because of concerns of high radioactivity from neutron-induced transmutation.[119]

Copper alloys are typically brazed at temperatures between 600 and 950 °C with hold times at the brazing temperature ranging from 10 s (torch, resistance, or induction brazing) to 10 min (furnace brazing).[2] The brazing process can significantly soften PH copper alloys as a result of the adverse precipitation process. To reduce the softening effect, a fast induction brazing technique has been developed to minimize the holding time at high temperature to retain sufficient mechanical properties.[120] Alternatively, the brazed component can be aged following furnace brazing to restore part of its initial strength. Complete recovery of high strength after furnace brazing by heat treatment in PH alloys is rather difficult in practice as the component must be heated to a temperature greater than typical brazing temperatures and rapidly quenched to create a supersaturation of solute prior to aging. Oxide DS copper has been successfully joined using torch, furnace, resistance, and induction brazing.[2] Softening is not a serious concern for the base metal of DS copper alloys because of their high recrystallization temperature. The brazed copper joints show good fatigue properties and relatively low ductility.[2]

Diffusion bonding is a viable technique to produce joints with high mechanical strength for DS copper alloys, but cannot be used to produce high-strength

joints in PH alloys because of significant softening of the base metal during high-temperature exposure. The DS CuAl15 and CuAl25 alloys can be joined by diffusion bonding with acceptable bond strengths under the diffusion bonding conditions similar to the normal HIPing conditions.[121]

Techniques for joining copper alloys to beryllium or austenitic stainless steels have been developed for the ITER plasma-facing components. A review of the joining technology was given by Odegard and Kalin.[119] Recent work has focused on small- and medium-scale mock-ups and full-scale prototypes of the ITER first wall panels.[122] The first wall panels of the ITER blanket are composed of a composite Cu alloy/316L(N) SS water-cooled heat sink structure with Be tile clad. A number of joining techniques have been explored for joining copper alloys to austenitic stainless steel, 316L(N), including diffusion bonding, brazing, roll bonding, explosive bonding, friction welding, and HIP.[123] HIP joining is by far the most desirable technique. For the PH CuCrZr alloy, the heat treatment must be integrated with the bonding cycle, and a high cooling rate ($>\sim$50 °C min^{-1}) is required to obtain good mechanical properties of CuCrZr after subsequent aging treatments. Two alternative processes are recommended[124]: the HIP cycle (1040 °C and 140 MPa for 2 h) followed by quenching in the HIP vessel, or a normal HIP cycle with a subsequent heat treatment in a furnace with fast cooling. Gervash *et al.*[125] studied alternative SS/Cu alloy joining methods, for example, casting, fast brazing, and explosion bonding. Cast SS/CuCrZr joint may be suitable for some ITER applications.

Brazing and diffusion bonding have been considered for joining the beryllium armor to a copper alloy heat sink. The Be/DS copper alloy joints can be made by high-temperature HIPing and furnace brazing.[126] Results from shear tests on small-scale specimens and from high heat flux tests of the first wall mock-ups showed good performance of joints brazed with STEMET 1108 alloy at $\sim$780 °C for less than 5 min.[122] The Be/Cu-Al25 solid HIPing (e.g., 730 °C and 140 MPa for 1 h) showed good performance from shear tests, high heat flux tests, and neutron irradiation.[122]

The development of joining techniques for PH CuCrCr alloy must consider the loss of mechanical strength because of overaging at high temperatures. The HIPing temperature must be reduced to be as close as possible to the aging temperature. The best results obtained so far is for HIPing at 580 °C and 140 MPa for 2 h.[126] A fast induction brazing technique has also been developed to minimize the holding time at high temperature. Diffusion bonding of Be/CuCrZr joints gives much better high heat flux performance than brazing, and has been selected as the reference method for the European Union ITER components.[120] A low-temperature Be/Cu alloy bonding process has also been developed that is compatible with both DS and PH copper alloys.[124,127] In the United States, several different joint assemblies for diffusion bonding a beryllium armor tile to a copper alloy heat sink have been evaluated.[128] To prevent formation of intermetallic compounds and promoting a good diffusion bond between the two substrates, aluminum or an aluminum–beryllium composite (AlBeMet-150) has been used as the interfacial material. Explosive bonding was used to bond a layer of Al or AlBeMet-150 to the copper substrate that was subsequently HIP diffusion bonded to an Al-coated beryllium tile. A thin Ti diffusion barrier (0.25 mm) was used as a diffusion barrier between the copper and aluminum to prevent the formation of Cu–Al intermetallic phases. The Be/Cu alloy joints showed good strength and failure resistance.

4.20.7 Summary

High heat flux applications for fusion energy systems require high-strength, high-conductivity materials. Selection of materials for high heat flux applications must consider thermal conductivity, strength and tensile ductility, fracture toughness, fatigue and creep–fatigue, and radiation resistance. Pure copper has excellent conductivity but poor strength. PH and DS copper alloys have superior strength and sufficient conductivity, and are prime candidates for high heat flux applications in fusion reactors. These two classes of alloys have their own advantages and disadvantages with regard to fabrication, joining, and in-service performance.

PH copper alloys, such as CuCrZr, are heat-treatable alloys. Their properties are strongly dependent on the thermomechanical treatments. They possess high strength and high conductivity in the prime-aged condition, and good fracture toughness and fatigue properties in both nonirradiated and irradiated conditions. However, this class of alloys is susceptible to softening at high temperatures because of precipitate overaging and recrystallization. Their properties can be significantly degraded during large component fabrication because of their inability to achieve rapid quenching rates. DS copper alloys such as GlidCop Al25 have excellent thermal stability, and

retain high strength up to temperatures near the melting point. The main disadvantages of this class of alloys are their relatively low fracture toughness and difficulty to join.

The effect of neutron irradiation in copper alloys depends largely on the irradiation temperature. At irradiation temperatures below ~300 °C, radiation hardening occurs along with loss of strain hardening capability and complete loss of uniform elongation. Radiation hardening saturates at about ~0.1 dpa in this temperature regime. At higher temperatures, radiation-induced softening can occur. Void swelling takes place between 180 and 500 °C, and the peak swelling temperature is ~300–325 °C for neutron irradiation at damage rates near 10^{-7} dpa s^{-1}. PH and DS copper alloys are more resistant to void swelling than pure copper. Irradiation slightly reduces the fracture toughness of copper alloys, and the effect is stronger in CuAl25 than in CuCrZr. Irradiation has no significant effect on fatigue and creep–fatigue performance. Transmutation products can significantly change the physical properties and swelling behavior in copper alloys.

Significant R&D efforts have been made to select and characterize copper alloys for high heat flux applications. The *ITER Material Property Handbook* provides a comprehensive database for pure copper, CuCrZr, and CuAl25. For the ITER first wall and divertor applications, CuCrZr has been selected as the prime candidate. Current focus is on fabrication, joining, and testing of large-scale components.

References

1. Butterworth, G. J.; Forty, C. B. A. *J. Nucl. Mater.* **1992**, *189*, 237.
2. Zinkle, S. J.; Fabritsiev, S. A. *Atomic and Plasma-Materials Interaction Data for Fusion (Supplement to the Journal Nuclear Fusion* **1994**, *5*, 163.
3. Davis, J. R., Ed. *ASM Specialty Handbook: Copper and Copper Alloys*; ASM International: Materials Park, OH, 2001; p 276.
4. Atrens, A.; Nairn, J.; Fernee, H.; FitzGerald, K.; Skennerton, G.; Olofinjana, A. *Mater. Forum* **1997**, *21*, 57.
5. Taubenblat, P. W.; Smith, W. E.; Graviano, A. R. In *High Conductivity Copper and Aluminum Alloys*; Ling, E., Taubenblat, P. W., Eds.; Metallurgical Soc of AIM: Warrendale, PA, 1984; p 19.
6. Lu, L.; Shen, Y.; Chen, X.; Qian, L.; Lu, K. *Science* **2004**, *304*, 422.
7. Hertzberg, R. W. *Deformation and Fracture Mechanics of Engineering Materials*, 4th ed.; Wiley: New York, 1995; p 142.
8. Kanno, M. *Zeitschrift fuer Metallkunde* **1988**, *79*, 684–688.
9. Suzuki, H.; Itoh, G.; *J. Japan Inst. Metals* **1984**, *48*, 1016.
10. Tang, N. Y.; Taplin, D. M. R.; Dunlop, G. L. *Mater. Sci. Technol.* **1985**, *1*, 270.
11. Kalinin, G.; Barabash, V.; Cardella, A.; *et al. J. Nucl. Mater.* **2000**, *283–287*, 10–19.
12. Edwards, D. J.; Singh, B. N.; Toft, P.; Eldrup, M. *J. Nucl. Mater.* **1998**, *258–263*, 978.
13. Edwards, D. J.; Singh, B. N.; Xu, Q.; Toft, P. *J. Nucl. Mater.* **2002**, *307–311*, 439.
14. Li, M.; Sokolov, M. A.; Zinkle, S. J. *J. Nucl. Mater.* **2009**, *393*, 36.
15. Singh, B. N.; Edwards, D. J.; Eldrup, M.; Toft, P. Risø-R-971(EN); Risø National Laboratory: Roskilde, Denmark, 1997.
16. Singh, B. N.; Edwards, D. J.; Eldrup, M.; Toft, P. Risø-R-937(EN) (Cu13); Risø National Laboratory: Roskilde, Denmark, 1997.
17. Singh, B. N.; Edwards, D. J.; Eldrup, M.; Toft, P. *J. Nucl. Mater.* **1997**, *249*, 1.
18. Singh, B. N.; Stubbins, J. F.; Toft, P. Risø-R-991(EN); Risø National Laboratory: Roskilde, Denmark, 1997.
19. Rioja, R. J.; Laughlin, D. E. *Acta Metall.* **1980**, *28*, 1301.
20. Guha, A. In *High Conductivity Copper and Aluminum Alloys*; Ling, E., Taubenblat, P. W., Eds.; The Metallurgical Society of AIME: Warrendale, PA, 1984; p 133.
21. Ageladarakis, P. A.; O'Dowd, N. P.; Webster, G. A. Tensile and fracture toughness tests of CuNiSi at room and cryogenic temperatures; JET-R (99)01, 1999.
22. Fabritsiev, S. A.; Pokrosky, A. S.; Zinkle, S. J.; Ostrovsky, S. E. *J. Nucl. Mater.* **2002**, *306*, 218.
23. Singh, B. N.; Edwards, D. J.; Toft, P. *J. Nucl. Mater.* **1996**, *238*, 244.
24. Singh, B. N.; Stubbins, J. F.; Toft, P. Risoe-R-1128(EN); Risoe National Laboratory: Roskilde, Denmark, 2000.
25. Zinkle, S. J.; Nesterova, E. V.; Barabash, V. R.; Rybin, V. V.; Naberenkov, A. V. *J. Nucl. Mater.* **1994**, *208*, 119.
26. Zinkle, S. J.; Horsewell, A.; Singh, B. N.; Sommer, W. F. *J. Nucl. Mater.* **1994**, *212–215*, 132.
27. *ASM Handbook:* Vol. 2, *Properties and Selection: Nonferrous Alloys and Special-Purpose Materials*; ASM International: Materials Park, OH, 1990; p 392.
28. Lide, D. R.; Kehiaian, H. V.; *CRC Handbook of Thermophysical and Thermochemical Data*; CRC Press: Boca Raton, FL, 1994; p 28.
29. Piatti, G.; Boerman, D. *J. Nucl. Mater.* **1991**, *185*, 29.
30. Zinkle, S. J.; Eatherly, W. S. *Fusion Materials Semi-annual Progress Report;* DOE/ER-0313/22; Oak Ridge National Laboratory, 1997; p 143.
31. Li, G.; Thomas, B. G.; Stubbins, J. F. *Metall. Mater. Trans. A* **2000**, *31A*, 2491.
32. Singh, B. N.; Edwards, D. J.; Horsewell, A.; Toft, P. Risø-R-839(EN) (Cu07); Risø National Laboratory: Roskilde, Denmark, 1995.
33. Singh, B. N.; Toft, P. Risø-R-1008(EN); Risø National Laboratory: Roskilde, Denmark, 1998.
34. Zinkle, S. J.; Eatherly, W. S. *Fusion Materials Semiannual Progress Report*; DOE/ER-0313/20; Oak Ridge National Laboratory, 1996; p 207.
35. Fabritsiev, S. A.; Rybin, V. V.; Kazakov, V. A.; Pokrovsky, A. S.; Barabash, V. R. *J. Nucl. Mater.* **1992**, *195*, 173.
36. Fabritsiev, S. A.; Pokrovsky, A. S. *J. Nucl. Mater.* **1997**, *249*, 250.
37. Fabritsiev, S. A.; Pokrovsky, A. S. *J. Nucl. Mater.* **1997**, *249*, 239.
38. Zinkle, S. J. *Fusion Materials Semiannual Progress Report for Period;* DOE/ER-0313/28; Oak Ridge National Laboratory, 2000; p 171.

39. Singh, B. N.; Edwards, D. J.; Tahtinen, S. Risø-R-1436 (EN); Risø National Laboratory: Roskilde, Denmark, 2004.
40. Edwards, D. J.; Singh, B. N.; Tahtinen, S. *J. Nucl. Mater.* **2007**, *367–370*, 904.
41. Holzwarth, U.; Pisoni, M.; Scholz, R.; Stamm, H.; Volcan, A. *J. Nucl. Mater.* **2000**, *279*, 19.
42. Ivanov, A. D.; Nikolaev, A. K.; Kalinin, G. M.; Rodin, M. E. *J. Nucl. Mater.* **2002**, *307–311*, 673.
43. Suzuki, H.; Kanno, M. *J. Japan Inst. Metals* **1971**, *35*, 434.
44. Toda, T. *Trans. Japan Inst. Metals* **1970**, *11*, 24.
45. Toda, T. *Trans. Japan Inst. Metals* **1970**, *11*, 30.
46. Edwards, D. J. Temperature and strain rate effects in high strength high conductivity copper alloys tested in air; *Fusion Reactor Materials Semiannual Progress Report;* DOE/ER-0313/23; Oak Ridge National Laboratory, **1997**; p 213.
47. Stephens, J. J.; Bourier, R. J.; Vigil, F. J.; Schmale, D. T. Sandia National Lab Report, SAND88-1351, 1988.
48. Alexander, D. J.; Zinkle, S. J.; Rowcliffe, A. F. *J. Nucl. Mater.* **1999**, *271–272*, 429.
49. Suzuki, R.; Saito, M.; Hatano, T. *Fusion Sci. Technol.* **2003**, *44*, 242.
50. Tahtinen, S.; Pyykkonen, M.; Karjalainen-Roikonen, P.; Singh, B. N.; Toft, P. *J. Nucl. Mater.* **1998**, *258–263*, 1010.
51. Nadkarni, A. V. In *High Conductivity Copper and Aluminum Alloys*; Ling, E., Taubenblat, P. W., Eds.; The Metallurgical Society of AIME: Warrendale, PA, 1984; p 77.
52. Broyles, S. E.; Anderson, K. R.; Groza, J. R.; Gibeling, J. G. *Metall. Mater. Trans.* **1996**, *27A*, 1217.
53. Leedy, K. D. Ph.D. Thesis, University of Illinois at Urbana-Champaign, Urbana, IL, 1997.
54. Singh, B. N.; Li, M.; Stubbins, J. F.; Johansen, B. S. Risø-R-1528 (EN); Risø National Laboratory: Roskilde, Denmark, 2005.
55. Li, M.; Stubbins, J. F. *J. ASTM Int.* **2005**, *2*, 251.
56. Li, M.; Singh, B. N.; Stubbins, J. F. *J. Nucl. Mater.* **2004**, *329–333*, 865.
57. Wu, X.; Pan, X.; Singh, B. N.; Li, M.; Stubbins, J. F. *J. Nucl. Mater.* **2007**, *367–370*, 984.
58. Tahtinen, S. Crack growth properties of unirradiated and irradiated CuAl25-IG0 and CuCrZr Alloys and HIP Joints with 316L(N)-IG0 Steel; ITER Doc. G73 RE 1298–05–26 F 1, 1997.
59. Nomura, Y.; Suzuki, R.; Saito, M. *J. Nucl. Mater.* **2002**, *307–311*, 681.
60. Zinkle, S. J. In *Effects of Radiation on Materials*, 15th International Symposium, ASTM STF 1125; Stoller, R. E., *et al.,* Eds.; ASTM: Philadelphia, PA, 1992; p 813.
61. Fabritsiev, S. A.; Zinkle, S. J.; Singh, B. N. *J. Nucl. Mater.* **1996**, *233–237*, 127.
62. Fabritsiev, S. A.; *et al. Fusion Materials Semi-annual Progress Report* for Period Ending December 31, 1995; DOE/ER-0313/19 (April 1996); 1996; pp 177–188.
63. Zinkle, S. J. *J. Phys. F Metals Phys.* **1988**, *18*, 377.
64. Edwards, D. J.; Singh, B. N.; Bilde-Sørensen, J. B. *J. Nucl. Mater.* **2005**, *342*, 164.
65. Zinkle, S. J.; Gibson, L. T. *Fusion Materials Semi-annual Progress;* Report DOE/ER-0313/27; Oak Ridge National Laboratory, **1999**; p 163.
66. Zinkle, S. J.; Victoria, M.; Abe, K. *J. Nucl. Mater.* **2002**, *307–311*, 31.
67. Fabritsiev, S. A.; Pokrovsky, A. S. *J. Nucl. Mater.* **2009**, *386–388*, 268.
68. Singh, B. N.; Edwards, D. J.; Toft, P. *J. Nucl. Mater.* **2001**, *299*, 205.
69. Fabritsiev, S. A.; Pokrovsky, A. S. *J. Nucl. Mater.* **2002**, *307–311*, 431.
70. Pan, X.; Wu, X.; Li, M.; Stubbins, J. F. *J. Nucl. Mater.* **2004**, *329–333*, 1088.
71. Fabritsiev, S. A.; Pokrovsky, A. S.; Zinkle, S. J.; *et al. J. Nucl. Mater.* **1996**, *233–237*, 526.
72. Tahtinen, S.; Pyykkonen, M.; Singh, B. N.; Toft, P. In *19th International Symposium on Effects of Radiation on Materials*, ASTM STP 1366; Hamilton, M. L., *et al.* Eds.; American Society for Testing and Materials: West Conshohocken, PA, 2000; p 1243.
73. Li, M.; Stubbins, J. F. *Fusion Sci. Technol.* **2003**, *44*, 186.
74. Leedy, K. D.; Stubbins, J. F.; Singh, B. N.; Garner, F. A. *J. Nucl. Mater.* **1996**, *233–237*, 547.
75. Singh, B. N.; Stubbins, J. F.; Toft, P. *J. Nucl. Mater.* **1999**, *275*, 125.
76. Srivatsan, T. R.; Anand, S. *Eng. Fract. Mech.* **1993**, *46*, 183.
77. Singh, B. N.; Tähtinen, S.; Moilanen, P.; *et al.* Risø-R-1571(EN); Risø National Laboratory: Roskilde, Denmark, 2007.
78. Ibragimov, S. S.; Aitkhozhin, E. S.; Pyatiletov, Y. S. In *13th International Symposium (Part II),* ASTM STP 956; Garner, F. A., Henager, C. H., Igata, N., Eds.; ASTM: Philadelphia, PA, 1987; p 5.
79. Jung, P. *J. Nucl. Mater.* **1993**, *200*, 138.
80. Pokrovsky, A. S.; Barabash, V. R.; Fabritsiev, S. A.; *et al. Fusion Materials Semi-annual Progress Report;* DOE/ER-0313/22; Oak Ridge National Laboratory, 1996; p 194.
81. Singh, B. N.; Horsewell, A.; Gelles, D. S.; Garner, F. A. *J. Nucl. Mater.* **1992**, *191–194*, 1172.
82. Witzig, W. F. *J. Appl. Phys.* **1952**, *23*, 1263.
83. Zinkle, S. J.; Farrell, K. *J. Nucl. Mater.* **1989**, *168*, 262.
84. Zinkle, S. J.; Farrell, K.; Kanazawa, H. *J. Nucl. Mater.* **1991**, *179–181*, 994.
85. Gamer, F. A.; Hamilton, M. L.; Shikama, T.; Edwards, D. J.; Newkirk, J. W. *J. Nucl. Mater.* **1992**, *191–194*, 386.
86. Zinkle, S. J.; Lee, E. H. *Metall. Mater. Trans.* **1990**, *21A*, 1037.
87. Zinkle, S. J.; Wolfer, W. G.; Kulcinski, G. L.; Seitzman, L. E. *Phil. Mag.* **1987**, *A55*, 127.
88. Mukouda, I.; Shimomura, Y.; Iiyama, T.; *et al. J. Nucl. Mater.* **2000**, *283–287*, 302.
89. Zinkle, S. J. *Fusion Reactor Materials Semiannual Progress Report;* DOE-ER-0313/3; Oak Ridge National Laboratory, 1987; p 86.
90. Xu, Q.; Yoshiie, T.; Sato, K. *J. Nucl. Mater.* **2009**, *386–388*, 363.
91. Edwards, D. J.; Anderson, K. R.; Garner, F. A.; Hamilton, M. L.; Stubbins, J. F.; Kumar, A. S. *J. Nucl. Mater.* **1992**, *191–194*, 416.
92. Gamer, F. A.; Brager, H. R.; Anderson, K. R. *J. Nucl. Mater.* **1991**, *179–181*, 250.
93. Edwards, D. J.; Newkirk, J. W.; Garner, F. A.; Hamilton, M. L.; Nadkarni, A. *Proceedings of the 16th ASTM International Symposium on the Effect of Radiation on Materials*, ASTM STP 1175, June 1992; Kumar, A. S., Gelles, D. S., Nanstad, R. K., Little, E. A., Eds.; 1994; p 1041.
94. Spitznagel, J. A.; Doyle, N. J.; Choke, W. J.; *et al. Nucl. Inst. Meth.* **1986**, *B16*, 279.
95. Gamer, F. A.; Brager, H. R.; Anderson, K. R. *J. Nucl. Mater.* **1991**, *179–181*, 250.
96. Singh, B. N.; Zinkle, S. J. *J. Nucl. Mater.* **1993**, *206*, 212.
97. Zinkle, S. J.; Knoll, R. W. *A Literature Review of Radiation Damage Data for Copper and Copper Alloys*; Report UWFDM-578; University of Wisconsin Fusion Technology Institute, June 1984.

98. Zinkle, S. J.; Matsukawa, Y. *J. Nucl. Mater.* **2004**, *329–333*, 88.
99. Ruhle, M.; Crump, J. C., III *Phys. Status Solidi A* **1970**, *2*, 257.
100. Zinkle, S. J.; Kulcinski, G. L.; Knoll, R. W. *J. Nucl. Mater.* **1986**, *138*, 46.
101. Eyre, B. L. *J. Phys. F Metal Phys.* **1973**, *3*, 422.
102. Luft, A. *Prog. Mater. Sci.* **1991**, *35*, 97.
103. Wechsler, M. S. In *The Inhomogeneity of Plastic Deformation*; Reed-Hill, R. E., Ed.; American Society for Metals: Metals Park, OH, 1972; p 19.
104. Greenfield, L. G.; Wilsdorf, H. G. F. *J. Appl. Phys.* **1961**, *32*, 827.
105. Diehl, J.; Hinzner, F. *Phys. Status Solidi* **1964**, *7*, 121.
106. Essmann, U.; Mader, S.; Seeger, A. *Z. Metallk.* **1961**, *52*, 443.
107. Essmann, U.; Seeger, A. *Phys. Status Solidi* **1964**, *4*, 177.
108. Sharp, J. V. *Phil. Mag.* **1967**, *19*, 77.
109. Sharp, J. V. In *Proceedings of the 4th European Regional Conference on Electron Microscopy*; Bocciarelli, D. D., Ed.; Rom, 1968; p 417.
110. Sharp, J. V. *Radiat. Eff.* **1972**, *23*, 181.
111. Howe, L. M. *Radiat. Eff.* **1974**, *23*, 181.
112. Adamson, R. B. *Phil. Mag.* **1968**, *17*, 681.
113. Adamson, R. B. *Acta Metall.* **1969**, *17*, 1169.
114. Sharp, J. V. *Acta Metall.* **1974**, *22*, 449.
115. Edwards, D. J.; Singh, B. N. *J. Nucl. Mater.* **2004**, *329–333*, 1072.
116. Johnson, E.; Hirsch, P. B. *Philos. Mag. A* **1981**, *43*, 157.
117. Robach, J. S.; Robertson, I. M.; Wirth, B. D.; Arsenlis, A. *Phil. Mag.* **2003**, *83*, 955.
118. Davis, J. R. Ed. *ASM Specialty Handbook: Copper and Copper Alloys*; ASM International: Materials Park, OH, 2001; p 276.
119. Odegard, B. C.; Kalin, B. A. *J. Nucl. Mater.* **1996**, *233–237*, 44.
120. Lorenzetto, P.; Boireau, B.; Boudot, C.; *et al. Fusion Eng. Design* **2008**, *83*, 1015.
121. Samal, P. K. In *The Metal Science of Joining*; Cieslak, M. J., Ed.; The Minerals, Metals and Materials Society: Warrendale, PA, 1992; p 295.
122. Lorenzetto, P.; Boireau, B.; Boudot, C.; *et al. Fusion Eng. Design* **2005**, *75–79*, 291.
123. Tsuchiya, K.; Kawamura, H. *J. Nucl. Mater.* **1996**, *233–237*, 913.
124. Sherlock, P.; Peacock, A. T.; McGallum, A. D. *Fusion Eng. Design* **2005**, *75–79*, 377.
125. Gervash, A.; Mazul, I.; Yablokov, N. *Fusion Eng. Design* **2001**, *56–57*, 381.
126. Lorenzetto, P.; Cardella, A.; Daenner, W.; *et al. Fusion Eng. Design* **2002**, *61–62*, 643.
127. Sherlock, P.; Peacock, A. T.; Rodig, M. *Fusion Eng. Design* **2007**, *82*, 1806.
128. Pukskar, J. D.; Goods, S. H.; Cadden, C. H. *Trends in Welding Research*, Proceedings of the 8th International Conference; David, S. A., DebRoy, T., DuPont, J. N., Koseki, T., Smartt, H. B., Eds.; ASM International, Materials Park, OH, 2009; p 604.